# Structural origin of sedimentary intrusions present in the AND-2A sedimentary rock core, Southern McMurdo Sound, Antarctica

Senior Thesis

Presented in partial fulfillment of the requirements for the

Bachelor of Science Degree

At The Ohio State University

By

Scott Robert Aleshire

The Ohio State University

May 2015

Approved by

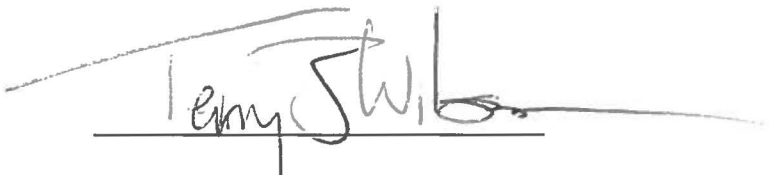

Terry J. Wilson, Advisor

School of Earth Sciences

## Abstract

This study examined the processes responsible for the formation of sedimentary intrusions, also known as clastic dikes, observed in the AND-2A sedimentary rock core from Southern McMurdo Sound, Antarctica. Logging of natural fractures in AND-2A provided the means to determine the relationship these structures have to larger regional structures, the Victoria Land Basin and the Transantarctic Mountains. Sedimentary facies analysis revealed variations in the proximity of grounded ice sheets to the depositional site of AND-2A strata in the western Ross Sea region. Formation of clastic intrusions in such a setting can be related to deformation of substrate beneath grounded ice, vertical loading of the crust by ice sheets, as well as stresses associated with tectonic activity. This study examined photos of various scales, made petrographic observation of thin section samples, plotted clastic dike attitude data and compiled sedimentary facies interpretations to determine the processes and drivers involved with clastic dike formation in AND-2A strata. Observation of clastic dike attributes indicates that many processes were involved with clastic injection in AND-2A. The formation of clastic dikes in AND-2A was driven by high fluid pressures in cohesive silty sediments, mostly diamictite lithologies. Water velocities supporting clastic injection in AND-2A varied during injection, and typically flushed finer grains away, leaving an average grain size of fine to medium sand within the dike margin. Various modes of grading within clastic dike margins suggest that both laminar and turbulent flow regimes operated at the time of injection. Lamination of intrusive material in AND-2A clastic dikes indicates variations in the velocity and viscosity of sand charged fluids, and alignment of grains parallel to clastic dike margins suggests the upward injection of sand material in AND-2A. Impermeable diamictites present in AND-2A allowed for the maintenance of high fluid pressures that are required for clastic

injection. Stereoplots and histograms of clastic dike orientation data suggest that a normal fault stress regime with significant differential stress operated at the time of their formation, and that clastic dikes formed after host sediments were largely compacted. Analysis of ice proximity to host strata at clastic dike sample depths showed that AND-2A clastic dikes form in ice-proximal to ice-distal depositional settings, and that while loading related to over-riding ice sheets likely contributed to the accumulation of overpressures, AND-2A clastic dikes can be attributed to tectonic activity in the VLB.

## Acknowledgments

I would first like to thank my family for their support during my undergraduate studies. In addition, I would like to thank the National Science Foundation for their funding of NSF OPP 0342484, ANDRILL–Investigating Antarctica's Role in Cenozoic Global Environmental Change and all of the people who worked on this project before me for providing the foundation that allowed me to do my work. Partial support for this research was provided by Shell Exploration and Production Company.

Dr. Terry Wilson deserves many thanks for her unending guidance throughout this project, for steering me in the right direction when I had no idea where to turn, and for her initial willingness to accommodate me into her research group.

Dr. Cristina Millan was an integral part of this journey. Her experience with the ANDRILL-SMS project and her willingness to help provided me with the materials needed for success in this project.

I would like to thank the rest of my coworkers in Dr. Wilson's research group for providing a fun and enjoyable atmosphere for me to complete my work.

I would also like to thank Ohio State's School of Earth Sciences's faculty and staff for making Mendenhall Laboratory a truly enjoyable place to be, specifically Dr. Lyons for supporting my initial interests in Antarctic research. Drs. Royce, Carey, and Panero deserve many thanks for their academic advising during my undergraduate career.

Finally, I would like to thank my girlfriend Hayley Howard for being a rock in my life, and for supporting me in whichever endeavors I choose.

# Table of Contents

## List of Figures

## List of Tables

## Introduction

The Antarctic Geological Drilling (ANDRILL) Project is a multidisciplinary project focused on retrieving and interpreting sedimentary rock cores to provide information on the climatic, glacial, and tectonic history of Antarctica. Specifically, the southern McMurdo Sound (SMS) Project sought to obtain sedimentary records from the middle Miocene, a time hypothesized to be fundamental in the development of modern-day Antarctic ice sheets (Florindo et al., 2008). The SMS project recovered an 1138 meter marine sedimentary record dating from the Pleistocene into the early Miocene from the Victoria Land Basin (VLB), which is filled with sediments derived from the Transantarctic Mountains (TAM) (Florindo et al., 2008). The SMS project complemented previous drilling experiments in Antarctica such as the McMurdo Ice Shelf Project, the Dry Valley Drilling Project and the Cenozoic Investigation in the Western Ross Sea Project. Sedimentary rocks in the AND-2A rock core provide the means to interpret Antarctic ice sheet variation in the Neogene, and provided Antarctic climate proxy data that could be integrated into global models (Florindo et al., 2008). Deposition of volcaniclastic rocks, derived from the Erebus Volcanic Province (EVP), in the sampled strata also allowed for understanding of the variability of Cenozoic volcanism in the region (Florindo et al., 2008). The sedimentary succession sampled in the AND-2A rock core provides the means for an intensive study of the relationships between tectonic, glacial, and climatic components of the dynamic Antarctic system (Florindo et al., 2008).

Figure 1 depicts a lithologic log of strata sampled by AND-2A, as well as a plot of natural fracture density in the AND-2A core. The logging of natural and induced fractures was completed to analyze tectonic structures in the core (Paulsen et al., 2008). Interpretations of

these macro-scale structures aided in understanding the role these features play in the past development and present day stress state of the West Antarctic Rift System (WARS). Natural fractures present in the core were logged and initially characterized as faults, veins, brecciation zones, and clastic dikes (Paulsen et al., 2008). A plot of clastic dike density in the AND-2A core is presented in Figure 2. While these structures have been generally logged and organized by type, observations from a smaller scale micro-analysis are required to interpret the processes and drivers responsible for the formation of clastic dikes during development of the VLB.

## *Study Objectives*

This project examined clastic dikes in the AND-2A core to contribute to an understanding of the processes and drivers of their formation in the Antarctic glaciated rift environment. In any setting, a variety of factors can cause clastic dike emplacement (Jolly and Lonergan, 2002). Through the observation of AND-2A clastic dike morphologies, intrusive materials, textures, host rocks, orientation, and the sedimentary facies in which they occur, this study sought to determine the processes that were in play during the formation of these features in the strata sampled by the AND-2A core. The findings of this study contribute to a multidisciplinary understanding of sediments and fractures logged in the AND-2A core, and provide information that can help discriminate whether clastic intrusions are markers of tectonic evolution, glacial history, or both, within the VLB.

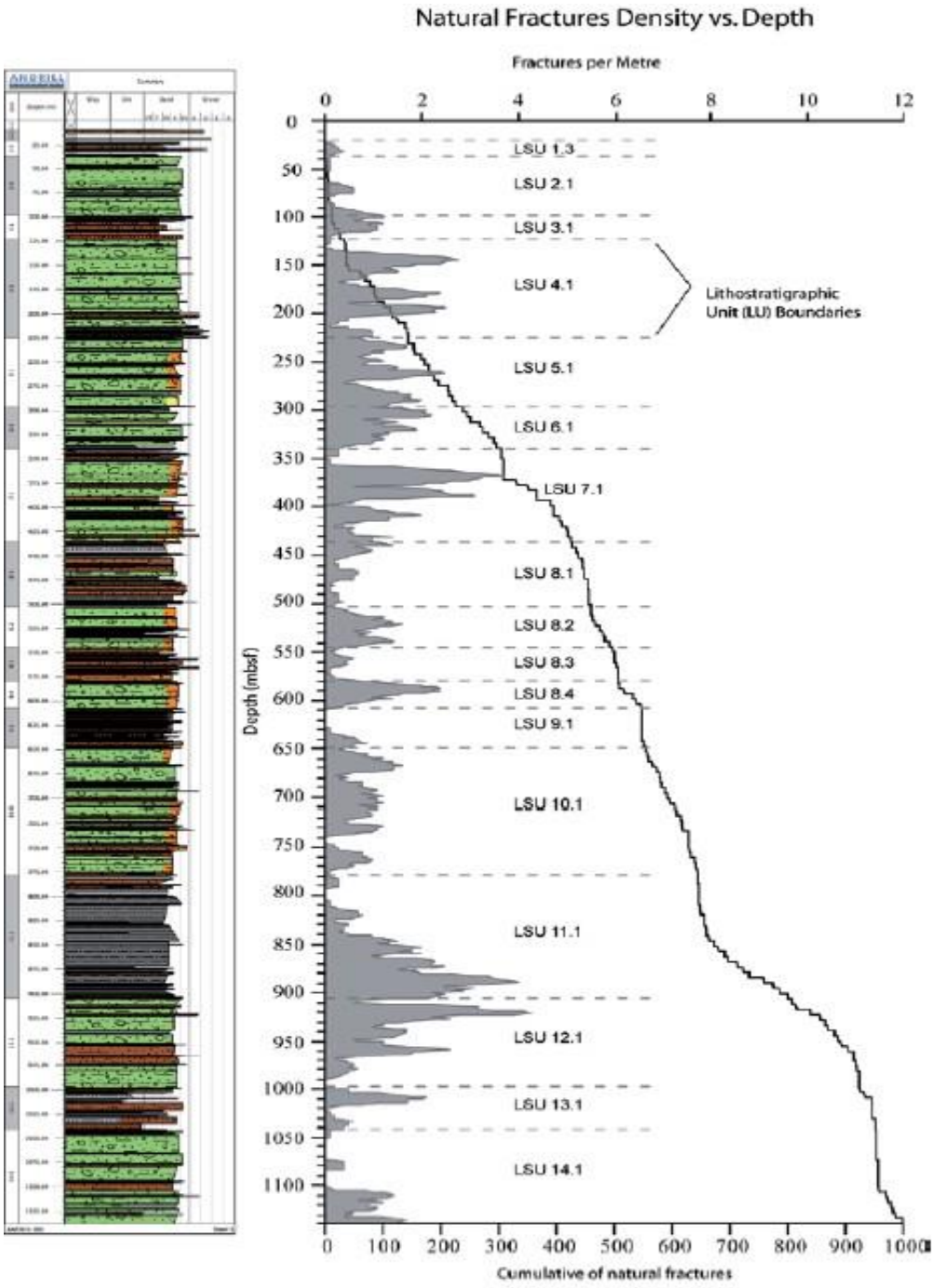


**Figure 1** (Left) Lithologic log of sedimentary rocks found in AND-2A, green indicates diamictite, brown indicates conglomerates, breccias and sandstones, and grey indicates mudstone lithologies. (Right) Plot of cumulative natural fracture density in the AND-2A core. This plot uses a 10 meter moving average to depict the number of natural fractures per meter of core as they relate to depth, lithology, and contact boundaries within the core (Paulsen et al., 2008).

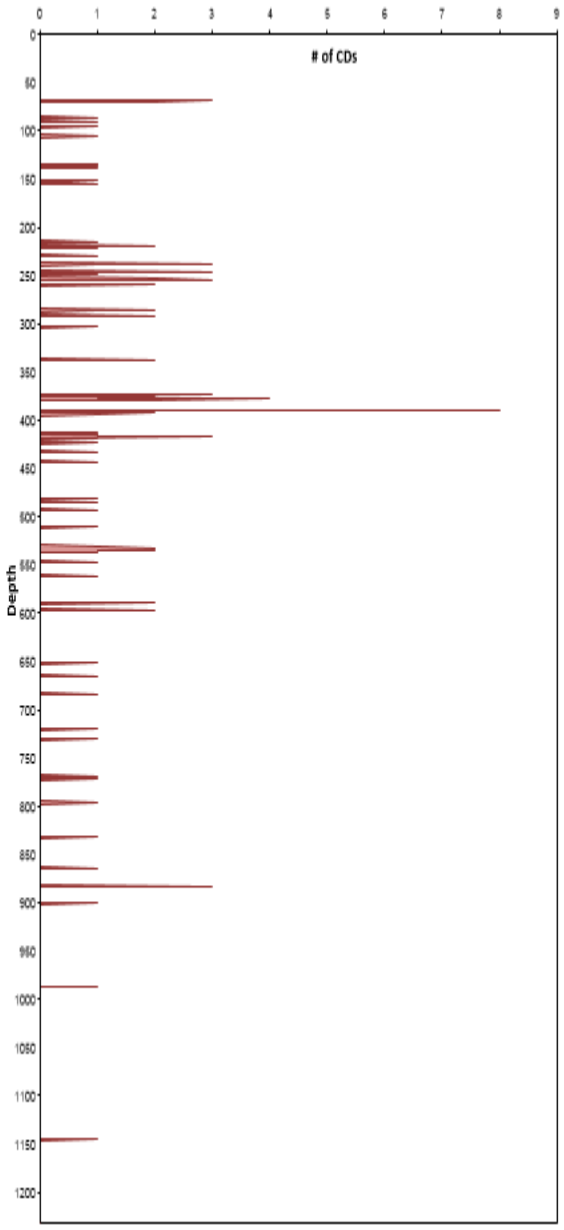


**Figure 2** Plot of CD density in the AND-2A core. This plot depicts the number of CDs logged in the AND-2A core vs. depth (provided by Cristina Millan).

## Geologic Setting

The AND-2A borehole was located in the southwest region of McMurdo Sound, adjacent to several key features of the Antarctic cryosphere and the West Antarctic Rift System (WARS) (Florindo et al., 2008). The core was drilled into Miocene sediments that filled the Victoria Land Basin, a 350-km long half-graben constituting the westernmost rift basin in the WARS (Florindo et al., 2008). Figure 3 details the location of the study area within Antarctica, with an inset showing regional tectonic features. Figure 4 provides an age model for the sedimentary rocks in the AND-2A core, showing that most of the strata sampled range in age from ~10-20 Ma. The VLB is one of several sedimentary basins in the Ross Sea, formed by crustal extension and subsidence since the breakup of Gondwana (Fitzgerald, 2002). To the west, the VLB is bordered by the Transantarctic Mountain (TAM) Front, a zone of major normal faulting creating the asymmetric tilt blocks of the TAM (Fitzgerald, 2002). These tilt blocks are divided by structures such as transfer faults or accommodation zones that are typically occupied by major outlet glaciers (Fitzgerald, 2002). Several major features of the Antarctic cryosphere operate in the vicinity of the borehole (Florindo et al., 2008). Facies analysis of sedimentary successions in the AND-2A core reveals highly variable glacial conditions in the regions surrounding McMurdo Sound throughout the early and middle Miocene (Fielding et al., 2011, Passchier et al., 2011). Ice mass variations in the East Antarctic Ice Sheet, the Ross Ice Shelf, the West Antarctic Ice Sheet, and sea-ice have all affected sedimentation in the VLB (Passchier et al., 2011).

Sedimentary rocks found in the AND-2A core are derived from erosion of the TAM, volcanism of the EVP, and biogenic production in McMurdo Sound (Fielding et al., 2011).

Figure 5 shows a satellite image noting the locations of the ANDRILL MIS and SMS project drill sites in the VLB, adjacent to the TAM, and a line of section A-A'. Figure 6 shows the structural cross section (A-A') across the TAM, the VLB and Ross Island with a large sedimentary wedge dipping eastward. Sediments are delivered via outlet glaciers of the East Antarctic Ice Sheet, eroding the TAM, or from the West Antarctic Ice Sheet and Ross Ice Shelf (Passchier et al., 2011).

Volcaniclastic rocks in the core are derived from Cenozoic rift-related volcanism in McMurdo Sound (Florindo et al., 2008). Subsidence related to normal faulting of the Terror Rift and volcanic loading have created accommodation space in the VLB from the Neogene into the Quaternary (Florindo et al., 2008). Sedimentation rates along the boundary between the TAM and the VLB have kept up with the rate of subsidence in the region, resulting in a 1.5–2 km thick wedge of strata, eroded off the TAM, whose thickness increases to 10 km moving eastward towards Ross Island (Florindo et al., 2008). Figure 7 shows a cartoon of the development of accommodation space in the VLB. Rift- and thermal-related subsidence, coupled with high sediment supply from the TAM, have provided the sedimentary record dating from the Pleistocene into the Early Miocene that is sampled in the AND-2A core.

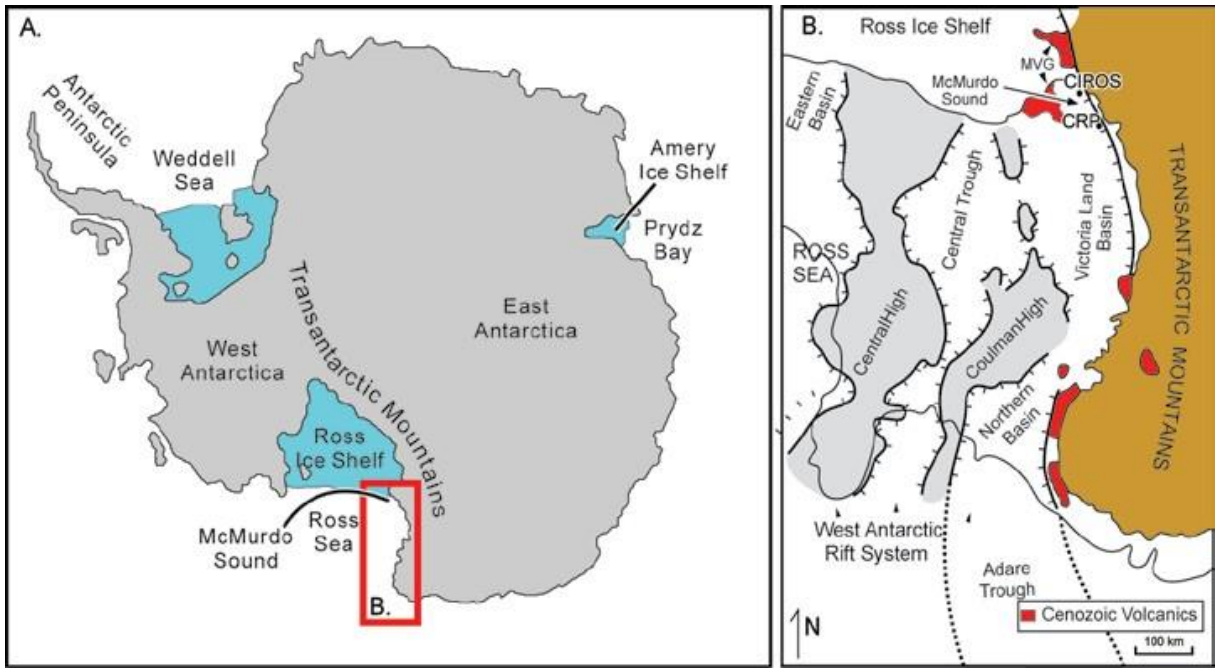


**Figure 3** Map A depicts the general location of McMurdo Sound in the western Ross Sea, close to the termination of the Ross Ice Shelf, and adjacent to the Transantarctic Mountains. Map B depicts regional highs and basins formed by tectonic activity (Florindo et al., 2008).

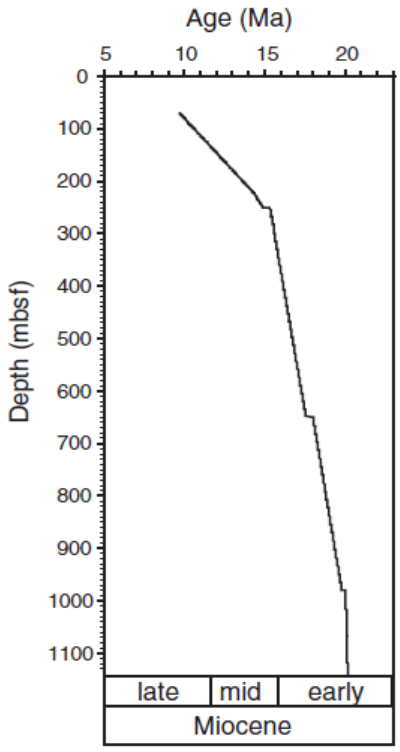


**Figure 4** Model for the age of sedimentary rocks in AND-2A core (Passchier et al., 2011).

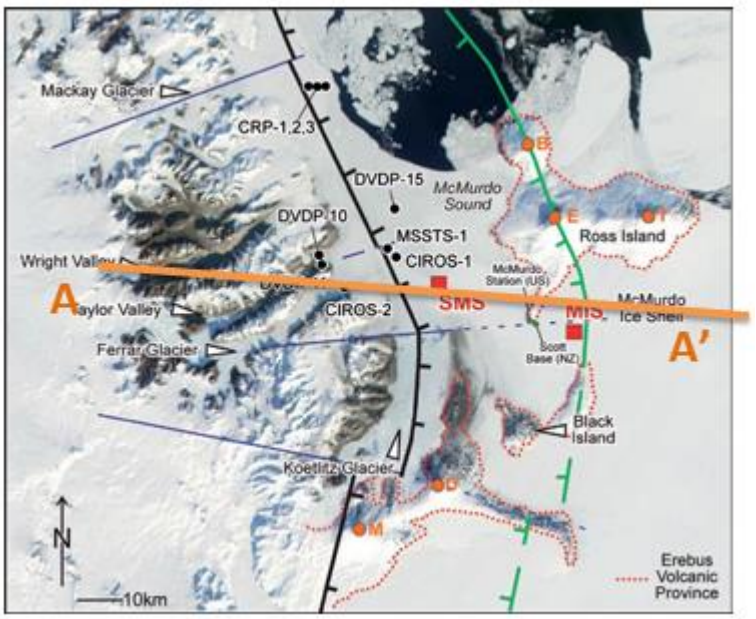


**Figure 5** Satellite image showing the relative locations of the MIS and SMS project drill sites in the Victoria Land Basin (Florindo et al., 2008). Includes line of section (A-A') in orange.

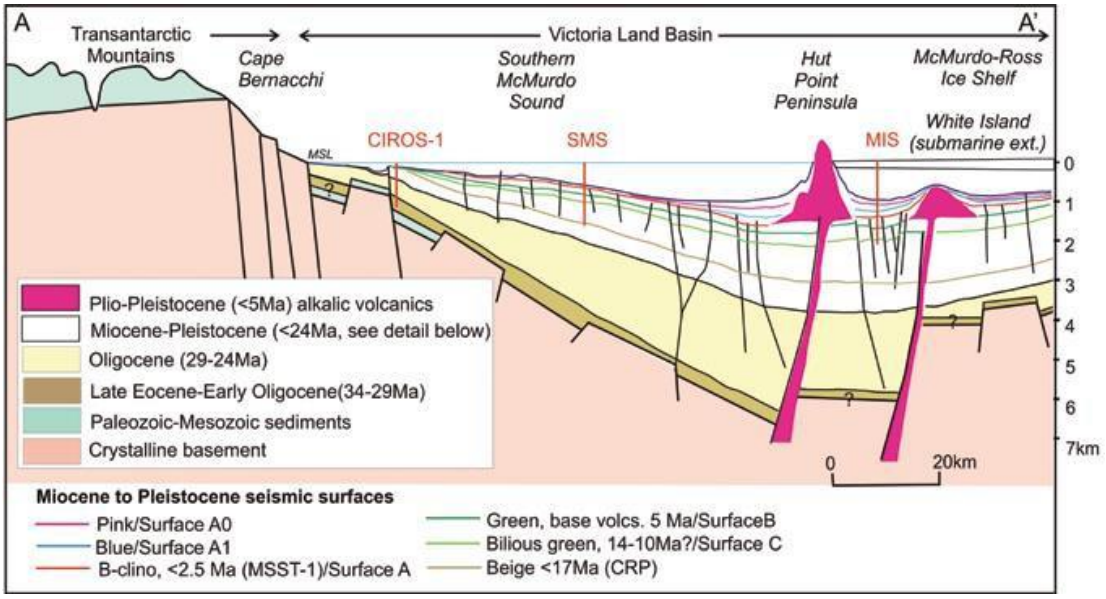


**Figure 6** Schematic structural cross section across the TAM, the VLB, and Ross Island, compiled from seismic reflection data, drill core data, and models interpreting the evolution of the VLB. Depicts stratigraphy relating to CIROS-1, MIS and SMS drill sites (Florindo et al., 2008).

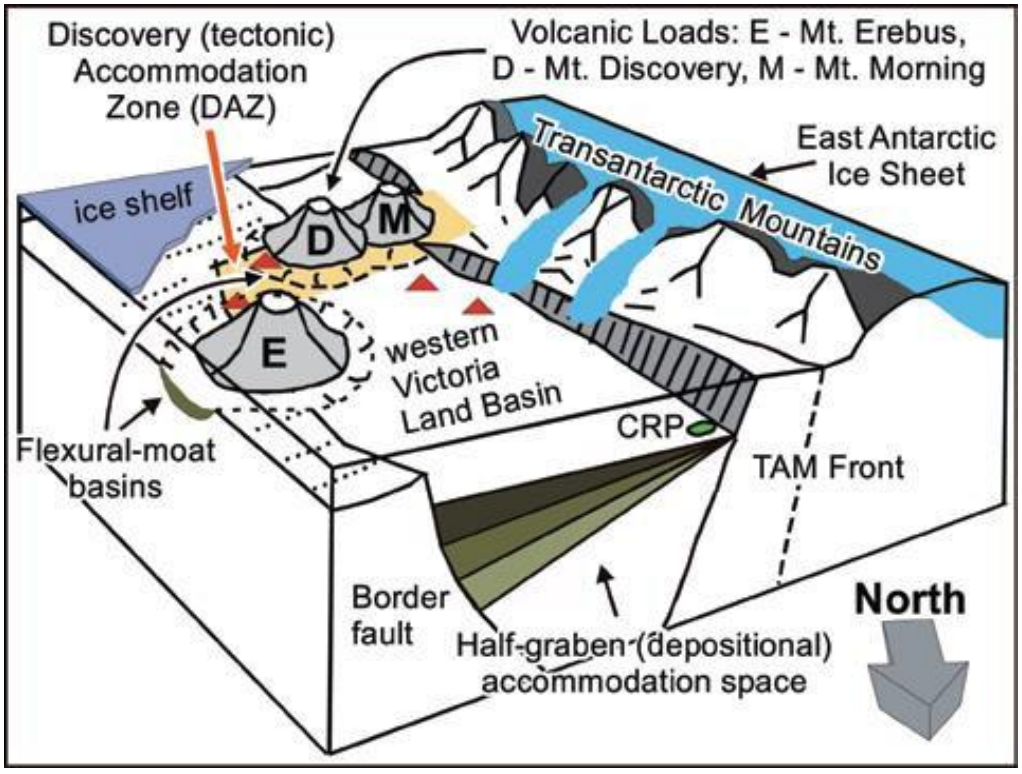


**Figure 7** Cartoon showing various components of the Antarctic system operating in the vicinity of ANDRILL drill sites (red triangles). (Florindo et al., 2008). Depicts the development of accommodation space in the VLB, adjacent to the TAM, with a sedimentary wedge dipping and thickening towards the east. Flexural moats developed as a result of volcanic loading, also providing accommodation space.

## Background on Clastic Dike Formation

Clastic dikes (CDs) have been documented in many sedimentary basins across the globe, on all seven continents, and are known to exist in nearly all depositional settings (Jolly and Lonergan, 2002). Figure 8 is a histogram of CD occurrence showing the wide range of depositional settings in which they can be found. While CDs have recently been recognized as central players in the process of diagenesis and the evolution of sedimentary basins around the globe, they remain poorly understood because their small-scale detail is not observable on seismic profiles (Huuse et al., 2010).

### *Soft Sediment Deformation Review*

**S**oft sediment deformation occurs prior to lithification, and provides a record of processes that affect unlithified sediments prior to, or very soon after, burial (Owen, 1987). The observation and interpretation of soft sediment deformation structures such as CDs have the potential to provide direct insight into the specific conditions that existed at the time of their formation (Mills, 1983). As a form of soft sediment deformation, structures related to CDs provide the most direct evidence for interpreting the processes that led to their formation (Hurst et al., 2011).

The deformation of unlithified sands can create a variety of soft sediment deformation structures (Cosgrove, 1995). With this diversity of structural characteristics, it is not surprising that CDs and their associated structures have been difficult to characterize systematically. Complicating this scenario is the fact that CDs are one point on a spectrum of other sand deformation structures that can occur if sediments are disturbed prior to complete lithification. Fluid escape structures such as dish and pillar structures, convolute lamination, load structures,

flame structures, and sand volcanoes are all related to the same processes that form CDs (Jolly and Lonergan, 2002).

### *Causes of Soft Sediment Deformation*

Soft sediment deformation can be caused by tectonics, glacigenic deformation, mass movements, or igneous activity (Owen and Moretti, 2011). Rapid sediment deposition, slope failure, breaking waves, and flood surges can all provide enough stress on unlithified sands for them to deform. In addition, cyclic triggers such as earthquakes, effects associated with freeze-thaw, pressure fluctuations associated with waves, and groundwater movements may also drive soft sediment deformation (Owen, 1987). While CD formation can be attributed to a variety of causes, seismicity and localized excess pore fluid pressures resulting from overburden are the most commonly cited triggers for CD formation (Jolly and Lonergan, 2002).

CDs caused by a seismic trigger have several distinguishing characteristics. Owen and Moretti (2011) cite lateral continuity, vertical repetition, proximity to faults active during sedimentation, and decreasing complexity of CD geometry with increasing distance from a fault as typical signs that a liquefaction event can be attributed to a seismic trigger. Characteristics of CDs caused by non-seismic triggers such as glacial processes are much harder to diagnose, as the criteria for trigger determination have not been intensively studied (Owen et al., 2011). However, van der Meer et al. (2009) cite a host of characteristics that are shared among CDs that formed in glacial settings: they are stepped in nature, they are widest at their intake, and they are typically finely laminated.

### *Process of Clastic Intrusion*

CDs are a result of the viscous flow of sand particles that have fluidized and subsequently filled mudstone fractures, and are therefore considered a form of natural hydraulic fracturing (Cosgrove, 2001). When mudstones are deposited, there is intrinsic cohesion between the particles of clay, and due to electrostatic forces between clay particles, they stick together (Hillier and Cosgrove, 2002). Sand grains do not have this inherent attraction to one another, and as a result, they are able to mobilize (Cosgrove, 2001). Increases in pore fluid pressure cause a reduction in the strength of the sediment bodies they affect, and if stress increases beyond strength of the material, it fractures, while unlithified sediments fluidize (Owen, 1987). If the applied stress increases to the point of mudstone failure, and there is a remaining pressure differential across the bed, the suspended sand grains will be injected upwards to fill the mudstone fractures (Jolly and Lonergan., 2002). Tensile fractures form parallel to the maximum principal compressive stress direction (Cosgrove, 1995). The spatial distribution of natural hydraulic fractures in rocks and sediments is controlled by the magnitude of the differential stress, the orientation of the principal stress axes, and the physical properties of the sediments they affect (Cosgrove, 1995). A generalized conceptualization of a zone affected by sand intrusion is provided in Figure 9.

The injection of CDs can be visualized as a three-step process, the accumulation of overpressure, mudstone (seal) failure, and subsequent fluidization and flow of a sand body into overlying strata (Jolly and Lonergan, 2002). Overpressure occurs when the pore fluid pressure in a layer of sediment is greater than hydrostatic or lithostatic pressure (Jolly and Lonergan, 2002). Overpressure typically accumulates in depositional environments where sand lenses are encased in low-permeability mudstones, which prevent the expulsion of fluids

from adjacent strata (Jolly and Lonergan, 2002). Overpressure can be accumulated through the transfer of pressure due to tectonic tilt, differential loading, mineral transformations related to diagenesis, cementation processes, and hydrocarbon generation (Huuse et al., 2010). Figure 10 shows a graph of overpressure increasing with depth. Seal failure, or the breaking of a mudstone cap rock, requires that the host sediments have some tensile strength, as is the case described in compacted mudstones with low permeability and the correct clay chemistry (Jolly and Lonergan, 2002). Figure 11 provides a visual depiction of different modes of seal failure, where the CD may form its own fracture, or may re-open previously existing fractures. Fluidization and subsequent entrainment of sand grains in a water flow require that the velocity of the flow exceeds the minimum fluidization velocity, the point where the upward force of fluid motion just balances the downward forces acting on the sand grains (Jolly and Lonergan, 2002). Figure 12 provides a conceptual diagram of how increases in pore fluid pressure eventually lead to fluidization of unlithified sediments. These injection events are interpreted to be relatively sudden events, as diffuse fluid seepage from sand bodies does not provide the pressure gradient required for fluids to reach the minimum fluidization velocity (Jolly and Longergan, 2002). Idealized scenarios associated with clastic injection are depicted in Figure 13.

While many CDs are interpreted to have injected upwards, a forceful mechanism such as this is not always required. Neptunian dikes can result from the passive infilling of a fracture or karst feature that is open at the surface (Jolly and Longergan, 2002). While these types of dikes are much less common, they have been reported by previous authors (Le Heron and Etienne, 2005).

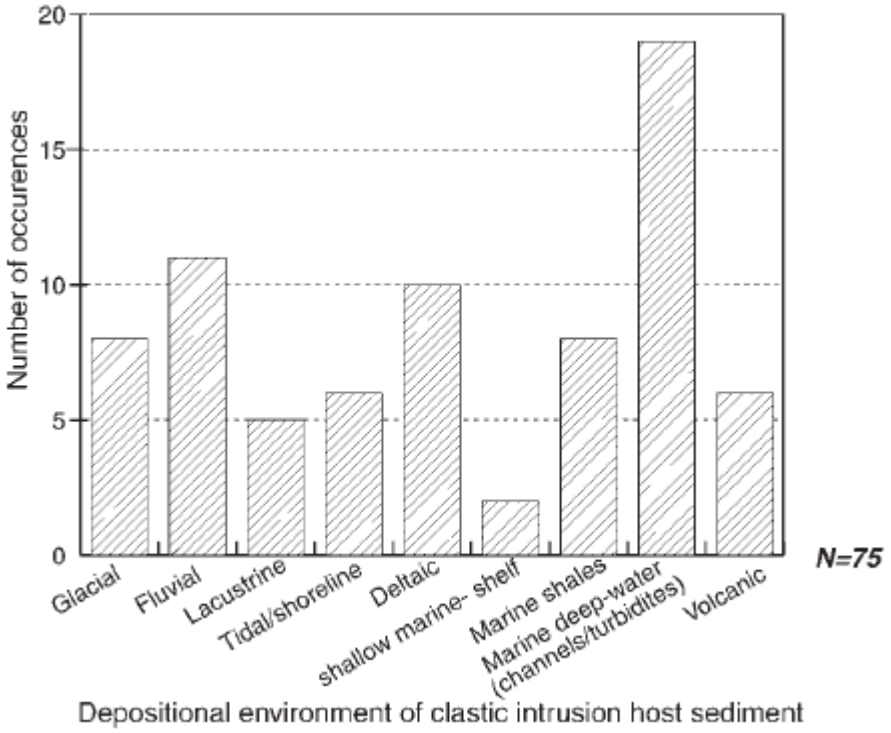


**Figure 8** Histogram compiling case study data that shows the variety of depositional environments CDs are found in (Jolly and Lonergan, 2002)

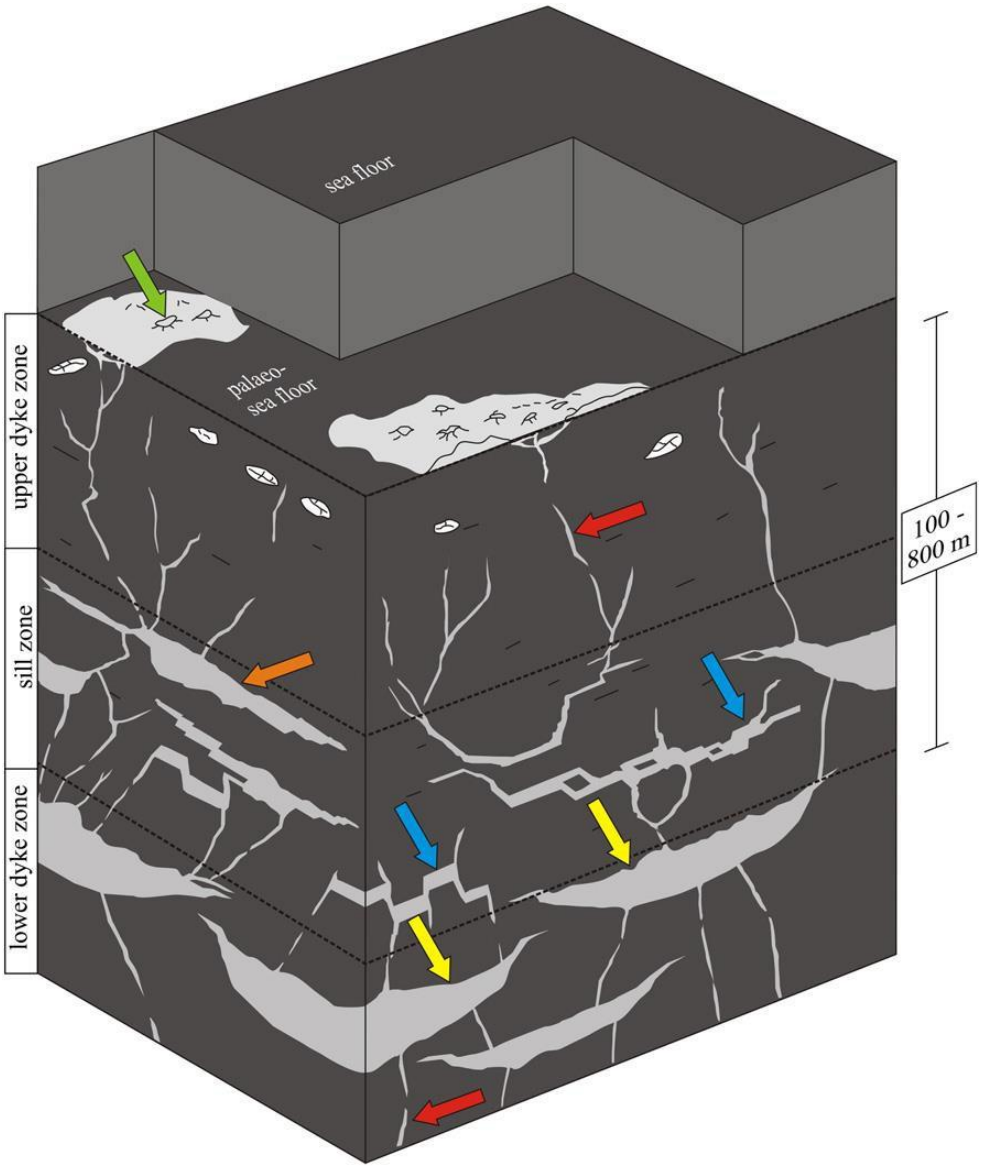


**Figure 9** A generalized diagram depicting a zone of clastic intrusion below the seafloor. The image shows the host rock (dark grey), remobilized parent sandstone units (yellow arrows), vertical sandstone dikes (red arrows), horizontal sandstone sills (blue arrows), irregular sandstone intrusions (orange arrow), with sandstone extrusions (green arrow) (Hurst et al., 2011).

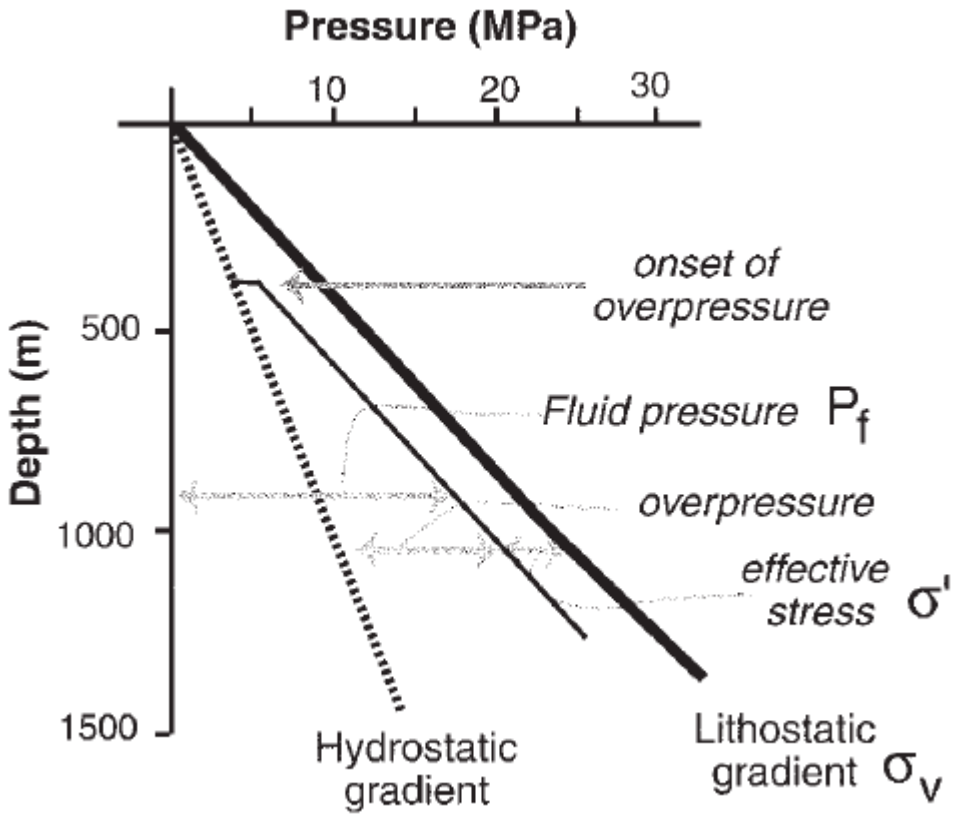


**Figure 10** Graph showing change in pressure with depth in a sedimentary succession. Shows increase of overpressure with depth (Jolly and Lonergan, 2002).

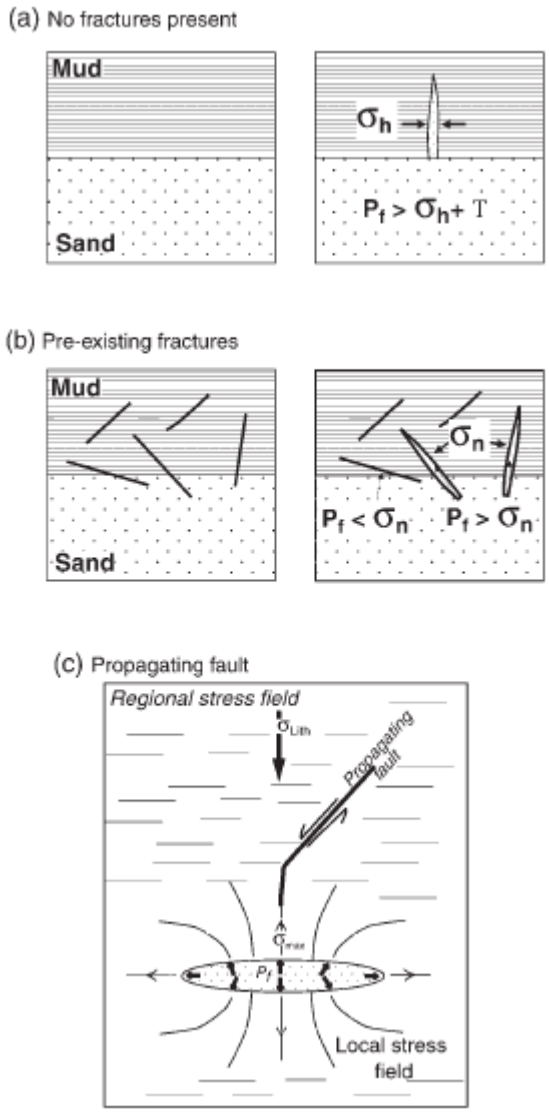


**Figure 11** Conceptual depiction of seal failure. (a) If there are no preexisting fractures, dikes will intrude normal to the least compressive principal stress. (b) If preexisting fractures are present, and fluid pressure exceeds normal stress on the fracture, sand will inject into these fractures. (c) A propagating fault may change orientation as a result of the changing stress field caused by overpressure and soft sediment related deformation (Jolly and Lonergan, 2002).

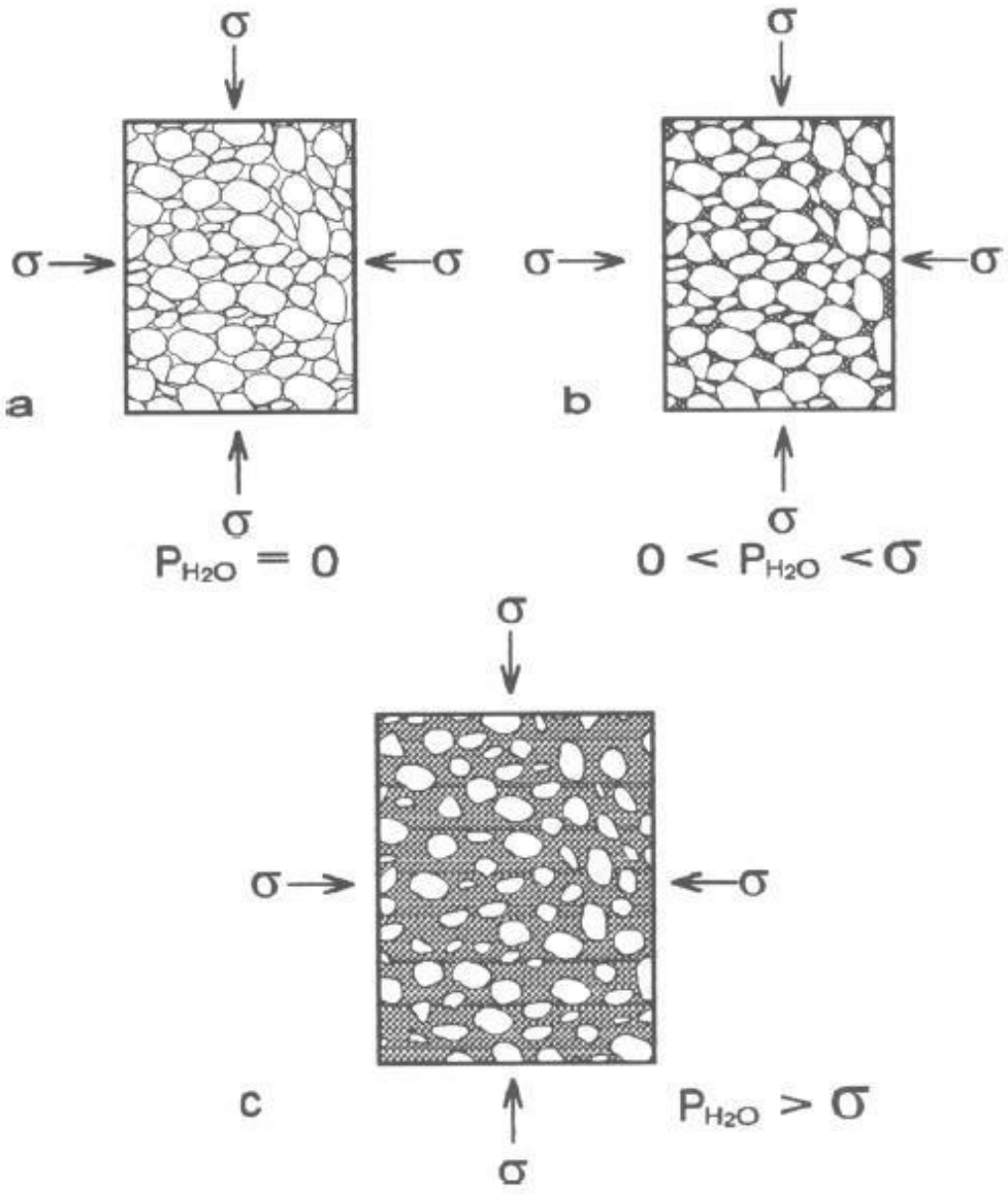


**Figure 12** Diagram of fluidization. (a) depicts the absence of fluid pressure in unlithified sandy sediments, and as pore fluid pressure increases in (b), space between the grains is taken up by fluids. If pore fluid pressure increases enough, as it does in (c), the sands will move apart even more, entraining particles of sand in the fluid (Cosgrove, 1995).

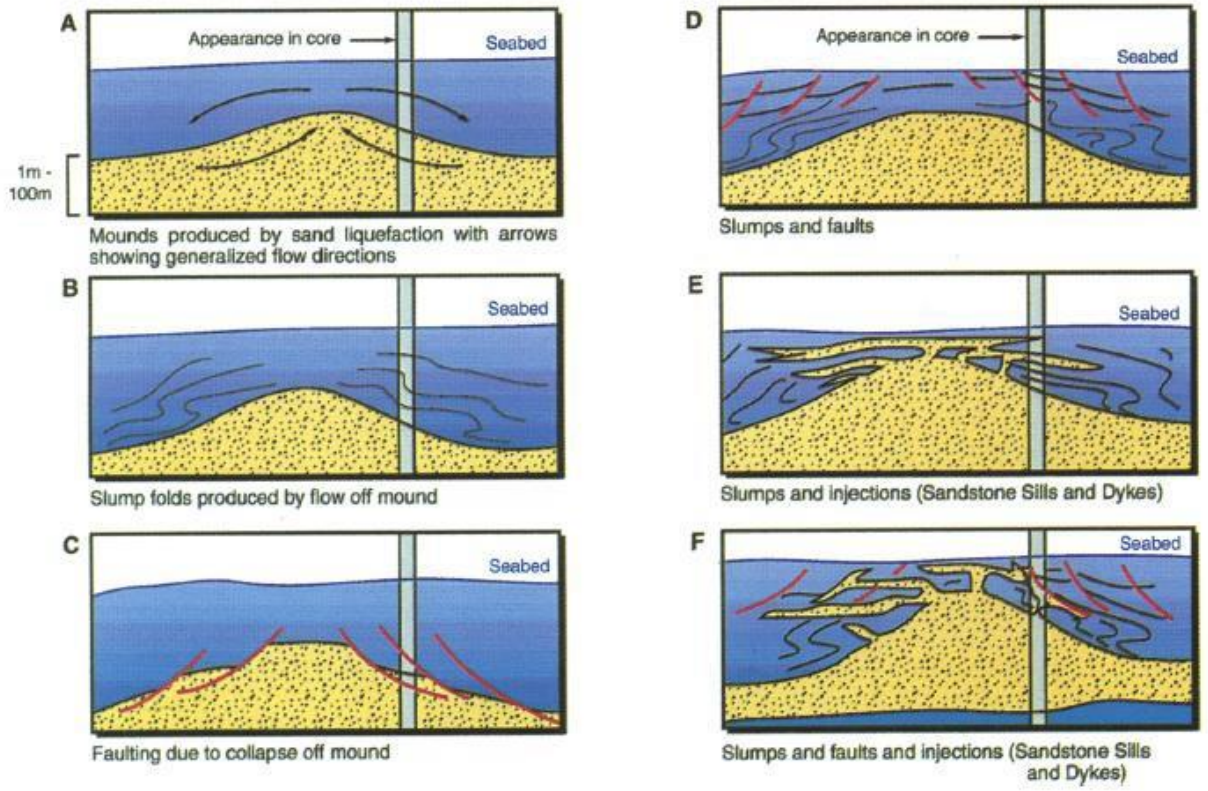


**Figure 13** Idealized scenarios associated with clastic intrusion. Blue colors represent cohesive mudstone sediments, and yellow colors represent sand. Deformation models developed by Dixon et al. (1995).

# Methods

## *Photo Analysis*

Prior to being cut in half, the outside of the AND-2A core was scanned using the CoreScan II instrument (Paulsen et al., 2008), resulting in whole-core images of the circumference of the core. After the core was split in half, scans of the resulting "half slabs" were taken. Scans of the thin sections were also made. For all samples examined in this study, images of all types and scales were edited using Adobe Photoshop. To make CDs more visible, contrast, brightness, and histograms of pixel values were modified. The images were then organized by sample and are presented in Appendix A. The whole-core and slabbed-core scans provide the larger scale, whole-core context for the microscopic observations made on thin sections. These photos were used to observe and characterize the larger scale geometry of the individual thin section samples that were interpreted to be CDs.

## *Petrographic Analysis*

Thin section samples were made representing the various types of natural fractures logged. Of the 1,000+ natural fractures logged in the core, 59 fractures were logged solely as either 'CD' or 'CD?'. This study used an Ortholux II POL-BK petrographic microscope to observe 13 thin section samples that were initially interpreted to have the characteristics of CDs. Observations detailing CD morphology, intrusive material, internal textures, and host rock characteristics were made and compiled into tables. A Wild M7 S microscope was used to observe grain shapes, grain sorting and features across entire CDs. Smaller scale features were photographed using a Leica DFC290 and the Leica Application Suite.

### *Orientation Analysis*

Fracture logging of the core included taking attitude measurements relative to an arbitrary core 'north'—a red scribe line drawn on the core soon after it was pulled out of the ground (Paulsen et al., 2008). Figure 14 shows the red scribe line and a blue scribe line 180 degrees away. When the core was split, it was cut perpendicular to the plane formed by these two lines (Paulsen et al., 2008). "Intact intervals" of core consist of core segments, separated by breaks, that can be fitted together without any internal rotation between the segments, so that all fractures within that interval are oriented with respect to one another (Paulsen et al., 2008). Figure 15 shows an intact interval with a continuity break and fitted fractures. Some intervals of core were able to be oriented to true north using magnetically-oriented borehole televiewer imagery (Paulsen et al., 2008). All fractures included in these "oriented intervals" are oriented with respect to true north.

This study aggregated orientation data based on intact intervals for any structure logged as 'CD' or 'CD?', even if it was logged as something like "F?V?CD?". If an intact interval containing CDs had breaks within the interval, a scribe match angle relating the two sections was applied to rotate the core segments to their correct orientation with respect to each other. If the intact interval was included in the portion of core that could be oriented to true north, a final rotation angle was used to rotate the orientation data to true north. This study used Stereonet 8.8.9 by R.W. Allmendinger, downloaded from http://www.geo.cornell.edu/geology/faculty/RWA/programs/stereonet.html, to plot CD attitude data for each intact interval (Appendix B). Planes plotted with a red line are CD thin section samples. Histograms of CD dip angle vs. depth and CD dip angle with 10 degree bins were compiled to evaluate patterns of CD dip distribution.

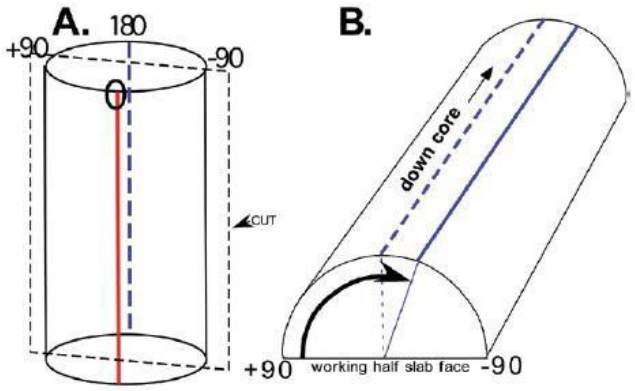


**Figure 14** Shows red scribe line used for core orientation indicating core 'north' (A), and a blue line 180 degrees from the red line (B). The core was split perpendicular to the plane formed by these two lines. If fractured, the angle between the red line on each adjacent core segment would be used to define a scribe match angle used to return the separate interval of core to its unbroken orientation (Paulsen et al., 2008).

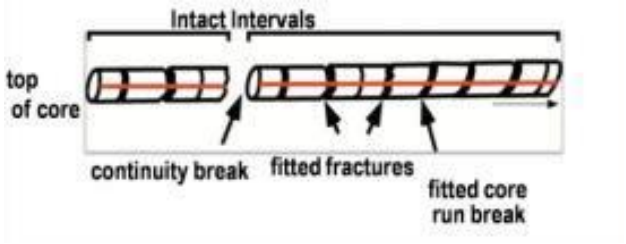


**Figure 15** Shows intact intervals with fitted fractures. Intact intervals are split by continuity breaks (Paulsen and Wilson, 1998).

### *Determining Proximity of Clastic Dike Host Strata to Subglacial Environments*

During core processing, sedimentary logs were compiled by Fielding et al. (2008). By depth, these logs detail various lithological units and primary sedimentary structures observed in the core. A list of structures occurring within 1 meter of CD thin section samples was compiled to explore the typical assemblage of structures occurring around areas of CD emplacement.

To determine glacial history of the regions surrounding McMurdo Sound, Passchier et al. (2011) and Fielding et al. (2011) performed facies analysis on the AND-2A core. In their analyses, the authors used different classification techniques, and separately interpreted depositional environments for sampled sedimentary strata in terms of grounded ice sheet proximity to the depositional site. In order to understand the potential role that over-riding ice sheets played in CD formation, ice proximity and facies interpretations at CD sample depths were compiled into color-coded charts to determine whether the strata containing a sampled CD was ice-proximal at the time of deposition or not. Figure 16 details facies divisions made by Passchier et al. (2011), and Figure 17 shows the facies the authors interpreted in AND-2A with CD sample depths listed. Figure 18 provides an explanation of depositional settings interpreted using their facies divisions. Figures 19 and 20 show the facies and motif divisions, respectively, used by Fielding et al. (2011). These divisions were used to create the log of AND-2A in Figure 21, with CD sample depths listed. Figure 22 details an idealized sequence of ice mass variation as interpreted by Fielding et al. (2011) from sedimentary rocks in AND-2A.

| Facies | Lithology | Structure | Clast (%) | Silica* (%) | Fossils† | Paleoenvironment |
|---|---|---|---|---|---|---|
| Z | Diatomaceous siltstone | Massive | <1–5 | 10–95 | Rare | Pelagic and hemipelagic with ice rafting |
| Zb | Siltstone | Bioturbated | Rare | <18 | Common | Hemipelagic with rare ice rafting |
| MSm | Muddy sandstone | Massive/laminated | <1 | <10 | Rare | Hemipelagic with significant ice rafting |
| Ss | Sandstone | Stratified | Rare | Trace | Rare | Wave- or current-influenced environment |
| SMs | Sandstone/mudstone | Interstratified | Rare | Trace | Rare | Ice-influenced delta top/front |
| SZs | Sandstone/siltstone | Interlaminated | <1 | Trace | Absent | Ice-proximal meltwater plumes |
| Ds | Diamictite | Stratified | 1–40 | Trace | Present | Ice-proximal to ice-distal glaciomarine |
| Dm | Diamictite | Massive | 1–40 | Trace | Rare | Ice-proximal glaciomarine or subglacial |
| G | Conglomerate/sandstone | Stratified/massive | >40 | Trace | Present | Ice-proximal glaciofluvial, ice-shelf collapse |

*Refers to biogenic silica content.
†Refers to calcareous macrofossils.

**Figure 16** Facies divisions defined by Passchier et al. (2011).

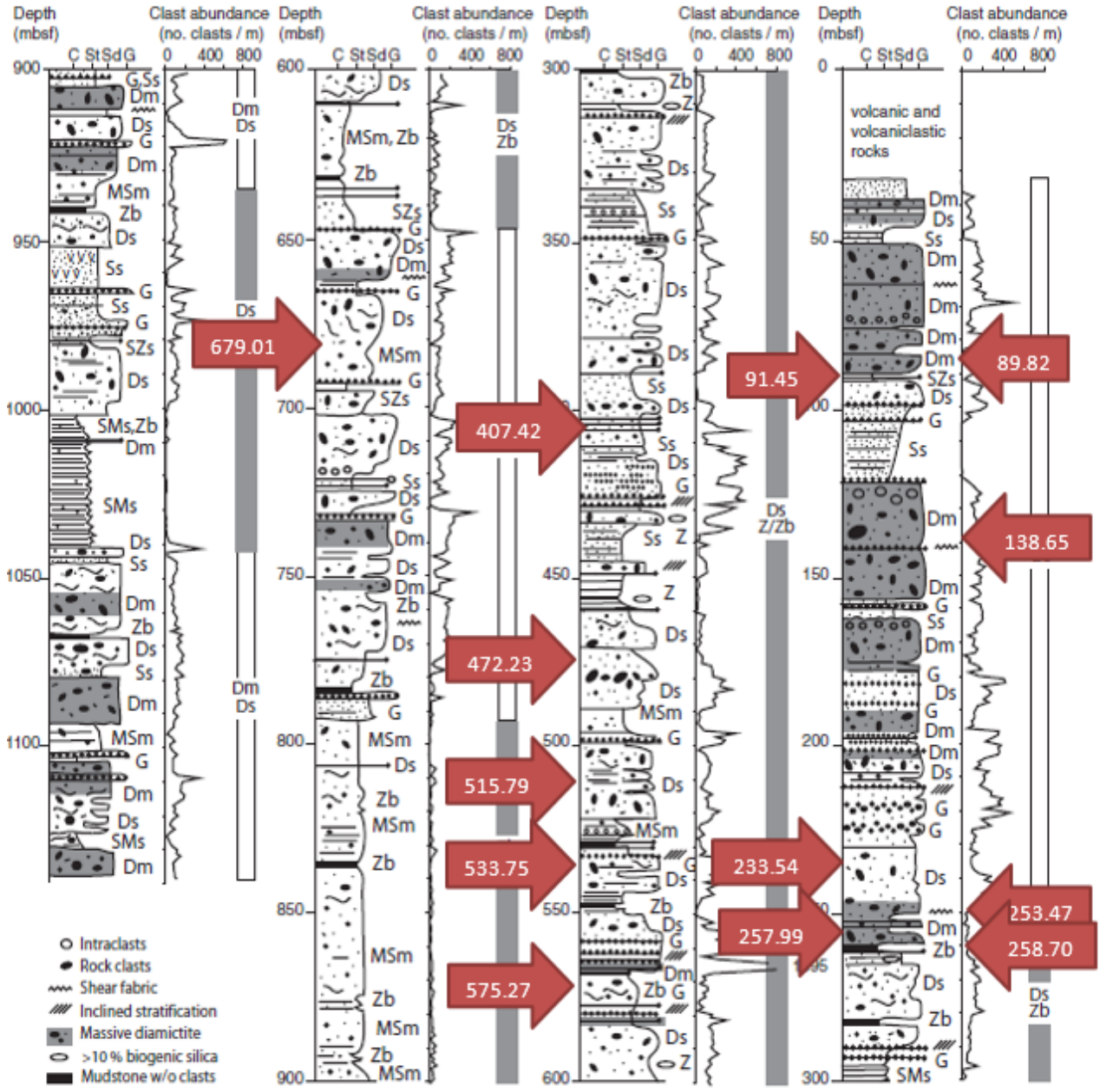


**Figure 17** Log of facies interpretations and clast counts per meter for AND-2A core. Diamictite-dominated intervals of core are shown using white bars, while stratified diamictite and mudstone dominated lithologies are shown using gray bars. Facies codes are explained in Figure 16 (Passchier et al., 2011). CD sample depths are indicated with red arrows.

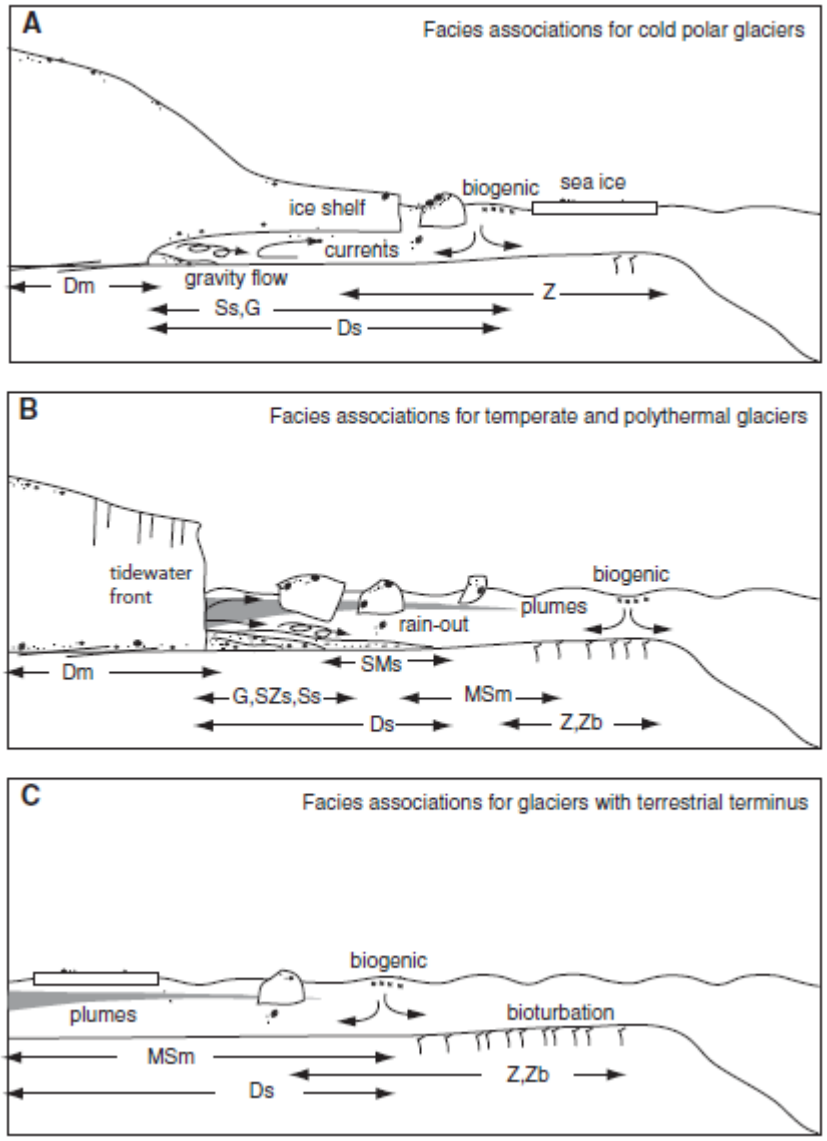


**Figure 18** Explanation of facies associations interpreted by Passchier et al. (2011). (A) near marine-based polar ice sheets, (B) near marine based temperate glaciers, and (C) near temperate ice sheets with a terminus on land.

| Facies | Description | Interpretation |
|---|---|---|
| 1 | Diatomite, opal-bearing or calcareous, fossil-rich mudstone, typically intensively and diversely bioturbated, little if any dispersed gravel | Open marine shelfal conditions (60–100 m water depth), minimal ice influence |
| 2 | Siltstone to very fine-grained sandstone, intensively and diversely bioturbated, dispersed small gravel and calcareous fossils, soft-sediment deformation structures | Open marine shelfal conditions (60–100 m water depth), deposition from suspension settling, distal ice influence |
| 3 | Interstratified siltstone and very fine- to fine-grained sandstone, bioturbated and/or stratified with ripple-scale structures, typically restricted and modest intensity bioturbation, dispersed calcareous fossils, soft-sediment deformation | Open marine to restricted coastal settings (10–80 m water depth), deposition from suspension settling, and gentle currents and waves, minor ice rafting |
| 4 | Stratified, fine- to coarse-grained sandstone, dispersed to locally concentrated small gravel, typically well sorted, with flat lamination, ripple cross-lamination, cross-bedding and hummocky cross-stratification, minimal bioturbation, locally fossiliferous | Open marine shoreface to upper offshore (10–40 m water depth), minor ice rafting of gravel |
| 5 | Muddy fine-grained sandstone to sandy siltstone with dispersed gravel, typically soft-sediment-deformed or unstratified, locally fossiliferous, rarely bioturbated | Open marine conditions (10–60 m water depth) affected by hemipelagic fallout and supply of sediment from ice-rafting |
| 6 | Delicately stratified, interlaminated fine- and coarse-grained siltstone, fine-grained sandstone and diamictite, dispersed gravel including diamictite clasts, some lamination rhythmic at sub-mm scale, soft-sediment and brittle deformation | Open glacimarine conditions affected by hemipelagic fallout, bottom currents and ice-rafting |
| 7 | Stratified diamictite, generally clast-poor, muddy to sandy matrix, commonly fossiliferous | Open, proximal glacimarine conditions, in distal portions of grounding-line fans |
| 8 | Massive diamictite, clast-poor to clast-rich and typically sandy matrix, some alignment of clast long-axes, shear structures including boxwork fracturing and brecciation | Ice-proximal glacimarine (grounding-line fan) to subglacial environments |
| 9 | Interbedded conglomerate and sandstone, thin units typically interbedded with other coarse-grained facies, locally fossiliferous | Ice-proximal environments in the presence of meltwater, various possible depositional settings |
| 10 | Vesicular, porphyritic, and basaltic lava | Primary sheet flows erupted from a proximal vent or fissure |
| 11 | Volcaniclastic breccias, monomict, composed of basaltic clasts in basaltic matrix | Autobrecciation of subaerially erupted lavas |
| 12 | Pyroclastic lapilli tuff, composed of glassy juvenile clasts of coarse ash to lapilli size | Settling of pyroclasts through the water column |
| 13 | Volcanic sedimentary breccias and sandstones, comprising texturally unmodified to modified juvenile volcanic clasts and grains, local ripple cross-lamination | Reworking of volcaniclastic deposits in shallow marine waters |

**Figure 19** Facies divisions defined by Fielding et al. (2011).

| Motif | Characteristics | Interpretation |
|---|---|---|
| 1 | Diamictite-dominated sequences, diamictites show shear and brecciation fabrics, are amalgamated, limited range and thickness of other lithologies | Cold, subpolar/polar glacial regime with minor meltwater involvement |
| 2 | Diamictite-dominated sequences, diamictites are more variable in character, are less amalgamated, greater range and abundance of other lithologies | Subpolar glacial regime with significant meltwater involvement |
| 3 | Sequences containing diverse lithologies including diamictites of varying character, sequences not diamictite-dominated | High-latitude temperate glacial regime, wet-based glaciers |
| 4a | Sequences containing basal diamictites but dominated by stratified sandstones | High-latitude temperate glacial regime, distant wet-based glaciers |
| 4b | Sequences containing basal diamictites but dominated by bioturbated and fossiliferous mudrocks | High-latitude temperate glacial regime, distant wet-based glaciers |
| 5 | Sequences containing thin basal diamictite or conglomerate but dominated by sandstones and mudrocks | Minimal (distal) glacial influence |

**Figure 20** Motif divisions defined by Fielding et al. (2011).

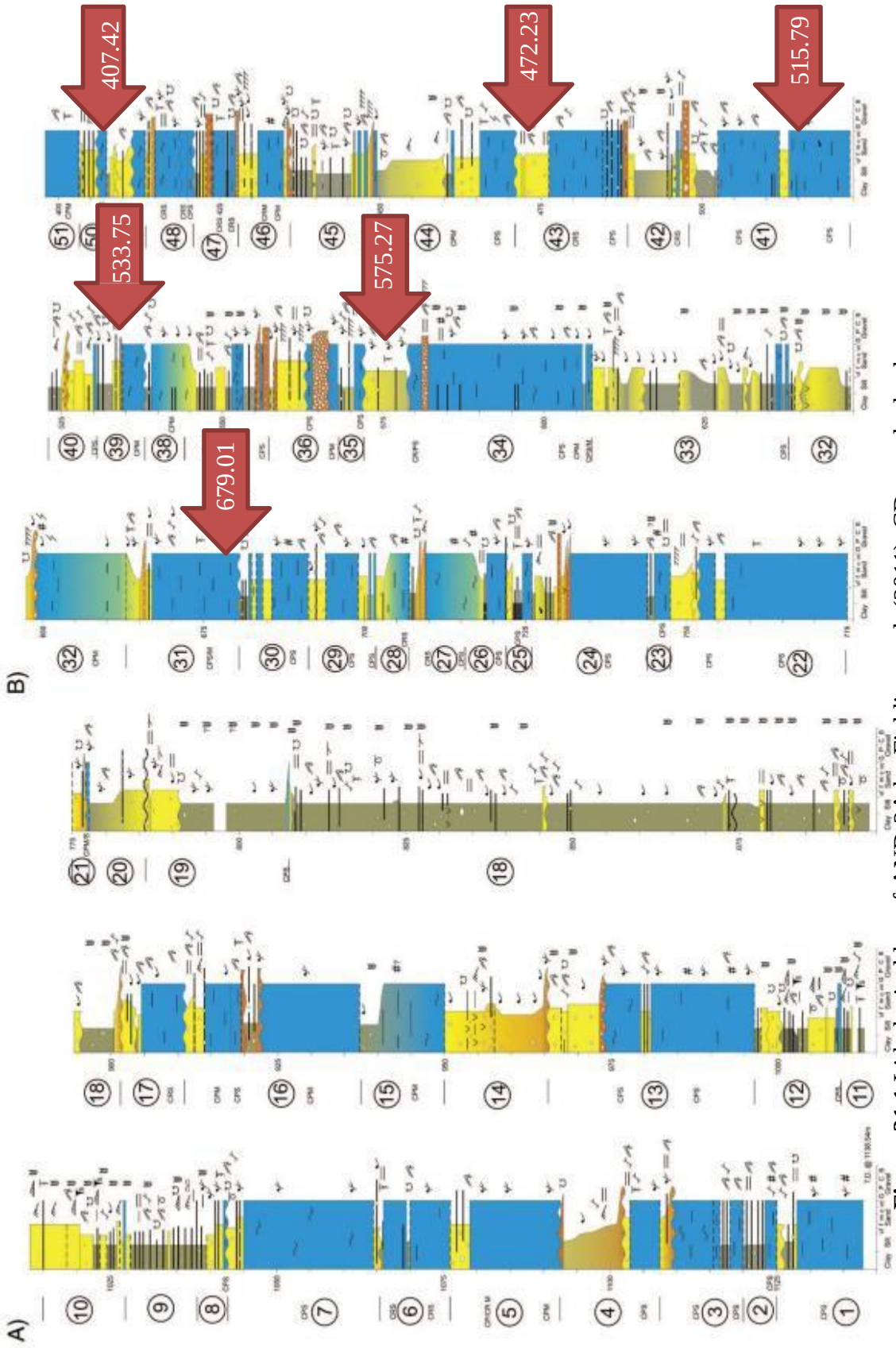


**Figure 21.1** Lithological log of AND-2A by Fielding et al. (2011). CD sample depths are shown in red. Gray-green indicates mudrock, yellow indicates sandstone, blue indicates diamictite, and orange indicates a conglomerate or breccia.

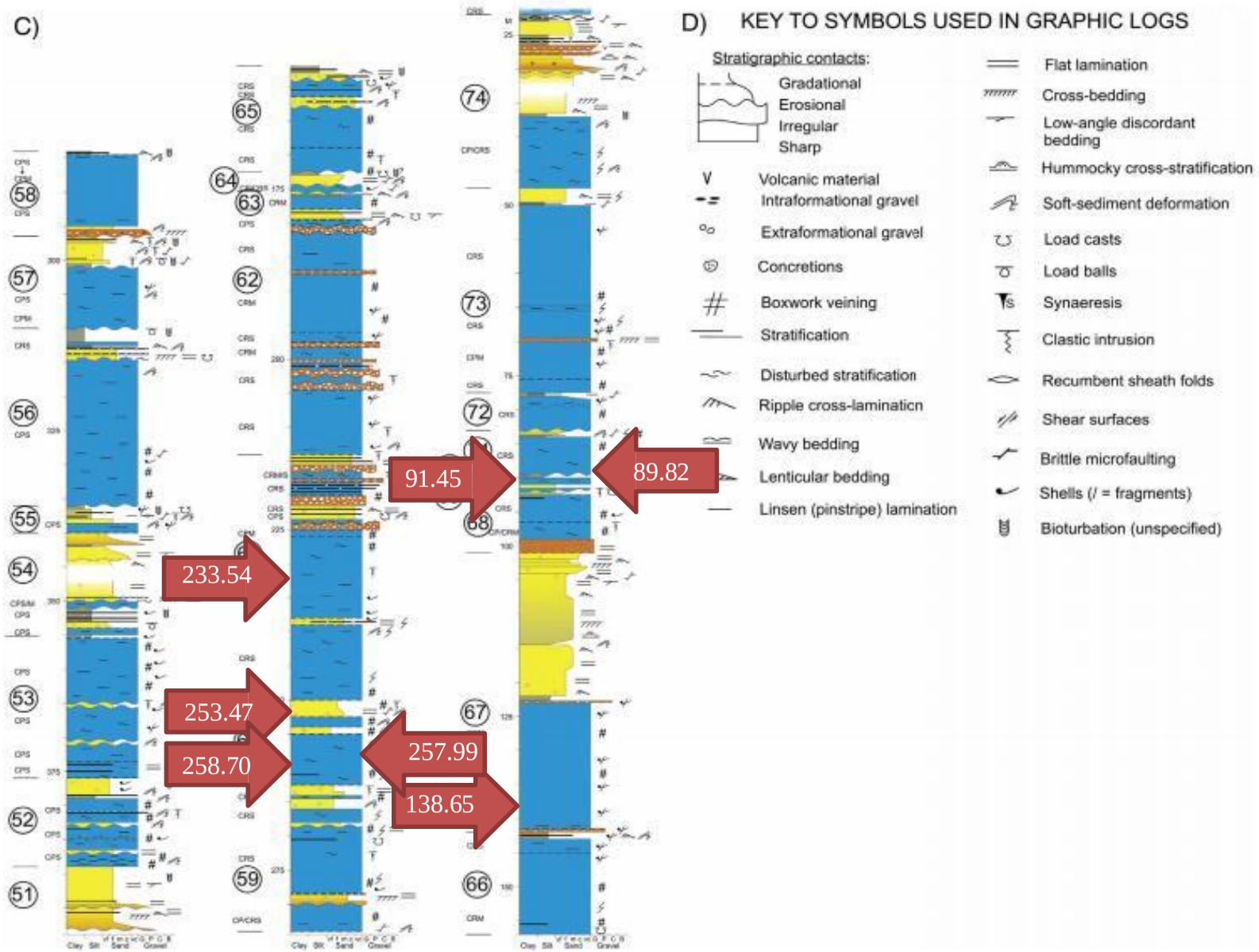


**Figure 21.2** Lithological log of ANDA by Fielding et al. (2011) cont'd.

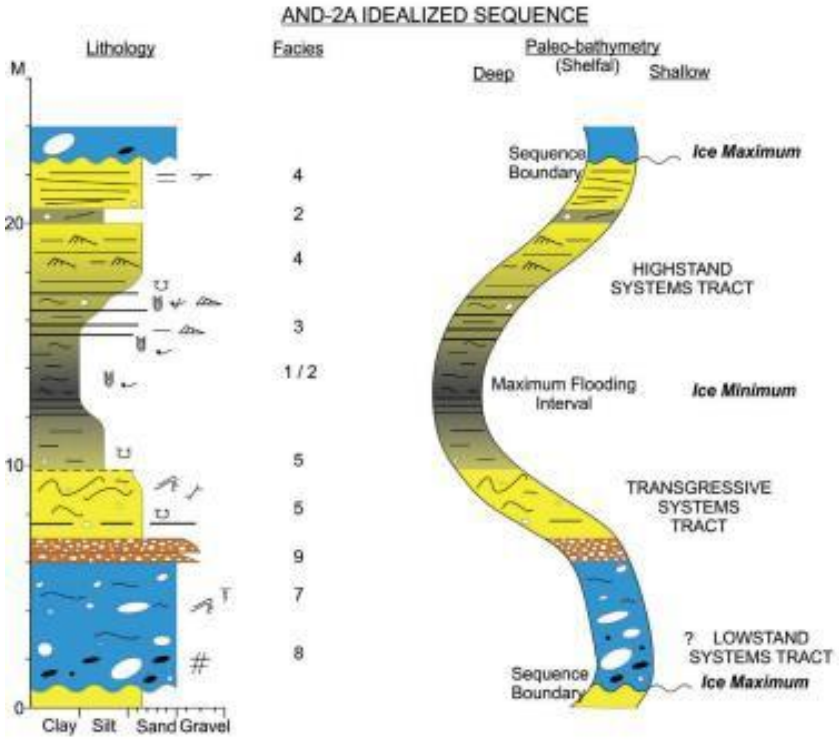


**Figure 22** An idealized sequence of ice mass variation interpreted from sedimentary rocks in AND-2A by Fielding et al. (2011), showing the interpretation of ice maxima and minima.

# Results

## *AND-2A Clastic Dike Morphology*

Table 1 details observations made on AND-2A CD morphology. CDs observed in thin section and using photos by Paulsen et al. (2008) show a wide variety of morphological characteristics. When observed in the core scans, morphology shows typically planar features 10s of millimeters to centimeters long, and less than 10 mm thick. They cross cut bedding (Figure 23), and are less than 10 mm thick measured perpendicular to the dike margins. In some cases, the CD appears to "zig zag", where a series of connected dikes and sills form a stepped pattern (Figure 24). Several other cases show the margin maintaining a wavy curved geometry instead of remaining completely planar (Figure 25). One CD was found to follow bedding completely for the entire length of the thin section sample, forming a "clastic sill". Others change orientation to follow bedding or to "wrap around" a clast.

Contacts between the CDs and the host rock show a variety of complex relationships. Sharp, distinct boundaries between the CD and the host rock are typical (Figures 23 & 26). Some CDs have one sharp and one diffuse margin on the opposite side of the dike. Some CDs are difficult to distinguish from the host rock, as the transition between the host rock and the CD interior is diffuse (Figure 24). In some cases, intrusive material greatly resembled the host rock and is mixed together with injected clastic material. Pyrite and clay alteration of the interior of the CD is very common (Figures 23, 24, 25, 26).

| Table 1 CD Morphology | | | | | | | | | |
|---|---|---|---|---|---|---|---|---|---|
| **Fracture #** | **Top Depth*** | Length as seen in core (mm)* | Length in thin section (mm) | Width perp. to margin (mm) | Planar Wavy , etc | At Bedding Plane | Contact w/ host rock | Alteration @ margin inside CD? | Structure near CD margin? |
| 400 | 89.82 | 48 | 23 | 2-3 | PL | CA | D | P | CD truncates bedding @ upper margin |
| 401 | 91.45 | 110 | 41 | 5-10 | PL | CA | D | CL | wide and then narrows, CD itself is offset by fault |
| 653 | 138.65 | 27 | 42 | 2-8 | W | follows | S | CL | lamination within CD, parallel to dike walls |
| N/A | 233.54 | --- | 30 | 5-7 | PL w/ S | ZZ | D, MU | P | CD itself forms sill, filling fracture along bedding plane |
| 1055b | 253.47 | 140 | 55 | 4-5 | PL w/ S | ZZ | S | CL | alteration halo outside of CD, connected clast-filled fractures formed around CD |
| 1061b | 257.99 | 520 | 45 | 1-2 | W | CA | S | P, CL | CD cross cuts mud layer, CD margin well defined through mud, less so through sand |
| 1064b | 258.7 | 170 | 37 | 5 | PL | CA | S | P | conjugate fracture outside of CD, clast filled fractures at bedding plane outside CD |
| 1505 | 407.42 | 120 | 25 | 3 | PL | CA | S & D | CL | distinct zone void of pyrite alteration within CD, pockets of clastic material outside CD |
| 1689 | 472.23 | 31 | 29 | 5-10 | quasi-PL | refracts | S & D | P | zone of "pinch out" in half slab, convolute bedding below CD in half slab |
| N/A | 515.78 | 54 | 48 | 2-5 | W | follows | D, MU | P, CL | CD itself is offset by fault |
| 1840 | 533.75 | 220 | 40 | 4-7 | PL | CA | S & D | CL | CD outlines clast, upper margin notably sharper than down core margin in CD |
| 1922 | 575.27 | 60 | 37 | 2-3 | PL | CA | S | -------- | broken fossils outside of CD |
| 2172 | 679.01 | 40 | 30 | 5-8 | W | CA | D, MU | CL | large clast comprised of sandstone inside CD |

| **LEGEND** | |
|---|---|
| PL-planar | D-diffuse |
| W- wavy | S- sharp |
| S- steps | MU-mixed up |
| CA-cuts across | P-pyrite |
| ZZ-zig zags | CL-clay |

**Table 1** Observations of CD morphology. *sourced from AND-2A fracture logs compiled by Paulsen et al. (2008).

### *Intrusive Material and Textures within AND-2A Clastic Dikes*

Table 2 details observations made on AND-2A CD intrusive material. The majority of intrusive material filling the CDs was observed to be quartz sand, ranging from medium to very coarse sand grain size (Figures 23 & 24). A limited number of CDs have intrusive material consisting of silt to very fine sand size. Opaque material and volcanic crystals are typically present, but in much lower concentrations. Pebbles and fossils are also observed within a few CD interiors. Few CDs show a low degree of sorting (Figure 25), with the majority of intrusive material moderately to very well sorted (Figures 23 & 26). Subangular and subrounded grains are equally common in the observed CDs, with only two CDs showing distinctly angular grains (Figure 24). One CD has sand grains so small that grain shape could not be discerned. Table 3 details observations made on textures within AND-2A CDs. Grading is present in the majority of CDs studied. The grain size of intrusive material commonly coarsens towards the center of the dike. Grain size variation across the width of the dike is also common. Grain size commonly gets larger up core (Figure 26). Coarsening down core occurred in one CD, and another is completely devoid of grading. In two CDs, alignment of clays and relatively elongate grains is strongly developed parallel to CD margins within the intrusion (Figure 26). In other CDs, relatively rounded grains did not define any clear alignment. In some cases, subrounded grains have very slight alignment (Figure 23). Lamination within the CD adjacent to the CD margin is very common in the sampled set of CDs (Figures 25 & 26). Lamination is parallel to the dike walls and is made up of clays or fine grained sand particles. In a few cases, laminae are observed within the CD. Some CDs showed no significant lamination inside the CD margin (Figure 23). Calcite and pyrite commonly constitute parts of the CD matrix. Clay is also observed as a form of secondary alteration, commonly forming pockets within the CD.

| Table 2 Intrusive Material | | | | | | | |
|---|---|---|---|---|---|---|---|
| **Fracture #** | **Top Depth *** | Max grain size | Avg grain size | Composition | Grain Shape | Grain Sorting | Cement/ Matrix in CD |
| 400 | 89.82 | VFS | Slt | 60% QS, 40% O | ------ | VW | C, P |
| 401 | 91.45 | FS | VFS | 60% QS, 40% O | A | M | C, CL |
| 653 | 138.65 | MS | Slt | 90% QS, 10% O | SA | W | P, CL |
| N/A | 233.54 | VCS | MS | 90% QS, 10% V | SA | M | Q, C |
| 1055b | 253.47 | VCS | FS | 90% QS, 10% O | SR | W | CL, C |
| 1061b | 257.99 | MS | VFS | 60% QS, 20% O, 20% V | SR | VW | C |
| 1064b | 258.7 | CS | MS | 80% QS, 10% O 10% V | SA | M | P, C |
| 1505 | 407.42 | MS | VFS | 90% QS, 5% O | A | VW | P |
| 1689 | 472.23 | CS | FS | 95% QS, 5% O | SA | M | P |
| N/A | 515.79 | CS | FS | 70% QS, 30% TS, | SR | P | P |
| 1840 | 533.75 | MS | FS | 90% QS, 5% O, 5% V | SR | M | CL, C |
| 1922 | 575.27 | VCS | MS | 85% QS, 10% O, 5% V | SR | VW | C, P |
| 2172 | 679.01 | CS | MS | 90% QS, 10% O | SA | P | C |

**LEGEND**

| | | | | |
|---|---|---|---|---|
| VF-very fine | Q/QS- quartz sand | A- angular | P-poor | C-calcite |
| F-fine | O- opaque | R-rounded | M-moderate | P-pyrite |
| M- medium | V- volcanic | SA-subangular | W-well | CL-clay |
| C-coarse | TS- too small/crystalline | | SR- subrounded | VW-very well |
| VC-very coarse | | | | |
| Slt- silt | | | | |
| S-sand | | | | |

**Table 2** Observations of CD intrusive material.
*sourced from AND-2A fracture logs compiled by Paulsen et al. (2008).

| Table 3 Textures within CD | | | | | | | |
|---|---|---|---|---|---|---|---|
| **Fracture #** | **Top Depth*** | Grain Shape | Grain Sorting | Grading inside dike? | Grain alignment ll to margin inside CD? | Lamination inside CD? | Alteration of grains/matrix? |
| 400 | 89.82 | ------ | VW | CTC | ------- | lamination of finer grained sand @ margin | pyrite |
| 401 | 91.45 | A | M | none | slight | none | calcite |
| 653 | 138.65 | SA | W | AW, CD | yes | apparent lamination of fine & coarse in dike | pyrite, clay |
| N/A | 233.54 | SA | M | CTC | slight | lamination of finer grained sand @ margin | pyrite |
| 1055b | 253.47 | SR | W | AW, CU | none | lamination of clay @ margin | clay |
| 1061b | 257.99 | S R | VW | none | slight | none | calcite |
| 1064b | 258.7 | SA | M | CTC | slight | none | pyrite |
| 1505 | 407.42 | A | VW | AW, CU | none | lamination of clay & finer grains @ margin | clay, pyrite |
| 1689 | 472.23 | SA | M | CTC | yes | lamination of fine & coarse grains @ margin | pyrite |
| N/A | 515.79 | SR | P | CTC | none | lamination of finer grains @ margin | pyrite |
| 1840 | 533.75 | SR | M | AW, CU | slight | coarse grains @ one margin, fines @ other | clay, calcite |
| 1922 | 575.27 | SR | VW | AW, CU | slight | none | calcite |
| 2172 | 679.01 | SA | P | none | none | none | clay, calcite |

| **LEGEND** | | |
|---|---|---|
| A-angular | VW-very well | AW- across width |
| SA-subangular | W-well | CTC- coarsens towards center |
| SR-subrounded | M-moderate | CU- coarsens up core |
| R-rounded | P-poor | CD- coarsens down core |

**Table 3** Observations of CD textures. *sourced from AND-2A fracture logs compiled by Paulsen et al. (2008).

### *Host Rocks*

Table 4 details observations made on AND-2A CD host rocks. The host rocks of observed CDs are ubiquitously cemented together with calcite. CDs typically occur in diamictites and sandstones of varying grain sizes. The diamictites typically have grain sizes ranging from silt to very coarse sand, with larger dispersed clasts present (Figure 23). Few diamictite lithologies where CDs occur have abundant clasts present. The sandstones in which AND-2A CDs occur are composed of fine sand, with some occurring as interlaminated siltstone and sandstone (Figures 24 & 26).

Table 5 compiles features logged in the core that occurred in the host strata in the vicinity of each CD studied. In AND-2A, CDs are most commonly observed in association with boxwork veins, flame structures, syneresis cracks and convolute bedding.

| **Table 4 Host Rock** | | | | |
|---|---|---|---|---|
| **Fracture #** | **Top Depth*** | Lithology | Grain size | Host rock cement |
| 400 | 89.82 | SltS SS IL | Slt-FS | C |
| 401 | 91.45 | SltS SS IL | Slt-FS | C |
| 653 | 138.65 | D | F-CS, AC | C |
| Not Logged | 233.54 | SltS- M SS | F-MS | C |
| 1055b | 253.47 | VB VF SS | Slt, DC | C |
| 1061b | 257.99 | D, SltS to M SS | Slt- MS, DC | C |
| 1064b | 258.7 | D, F-C SS | F-CS, DC | C |
| 1505 | 407.42 | VB SS | Slt- F S, DC | C |
| 1689 | 472.23 | VF-C SS IL | Slt- CS | C |
| Not Logged | 515.79 | VB D, SS | F-CS | C |
| 1840 | 533.75 | F-C SS | VF-CS, AC | C |
| 1922 | 575.27 | VB VF-C SS | Slt-CS | C |
| 2172 | 679.01 | D | VF-VCS, DC | C |

| **LEGEND** | |
|---|---|
| VF-very fine | IL- interlaminated |
| F-fine | D- diamictite |
| M-medium | VB- volcanic bearing |
| C-coarse | AC- abundant clasts |
| VC- very coarse | DC- dispersed clasts |
| Slt- silt | C- calcite |
| S-sand | |
| SltS- siltstone | |
| SS- sandstone | |

**Table 4** Observations of host rocks. *sourced from AND-2A fracture logs compiled by Paulsen et al. (2008).


**Figure 23** Fracture 1064b at 258.70 mbsf.

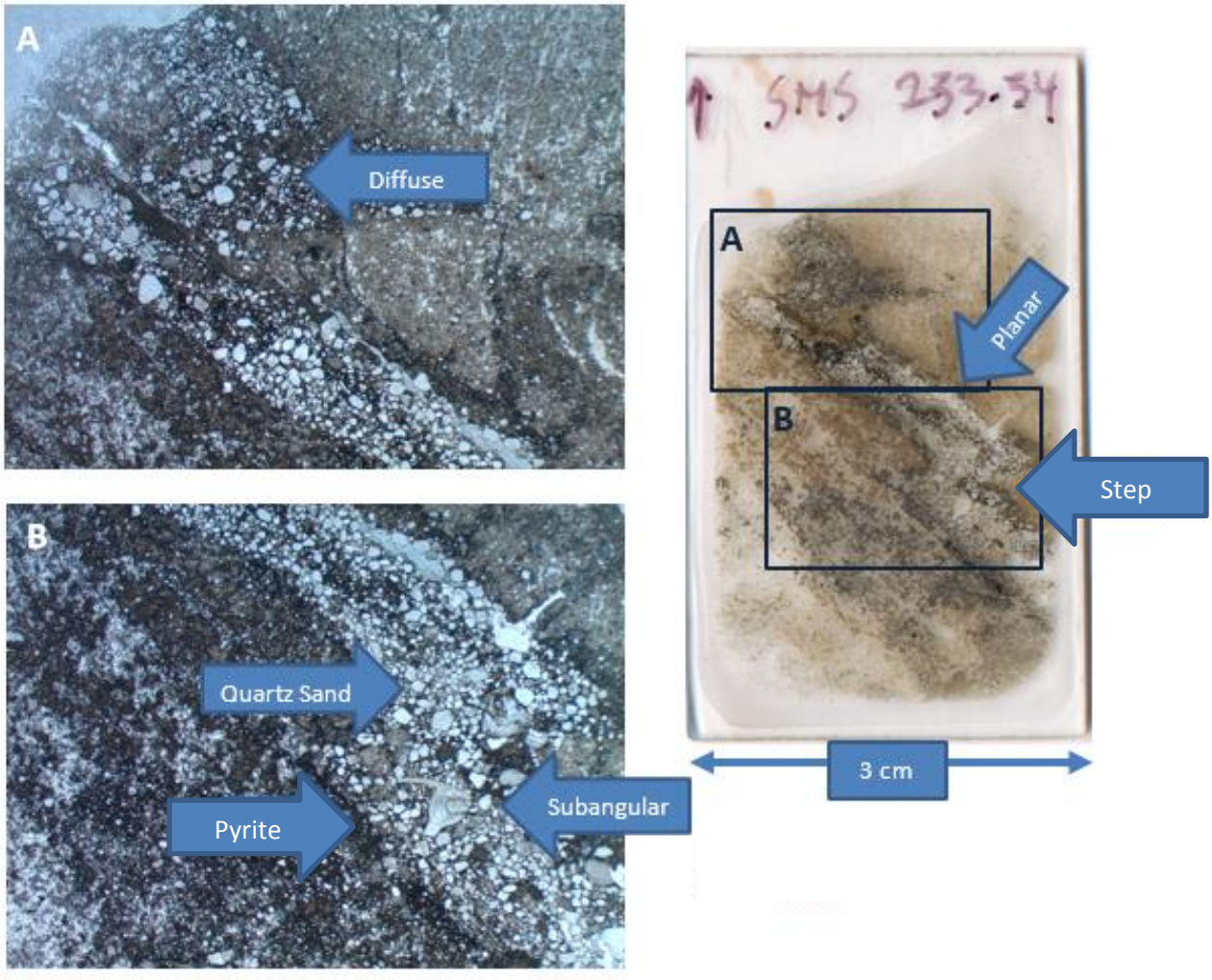


**Figure 24** Unlogged fracture at 233.54 mbsf.

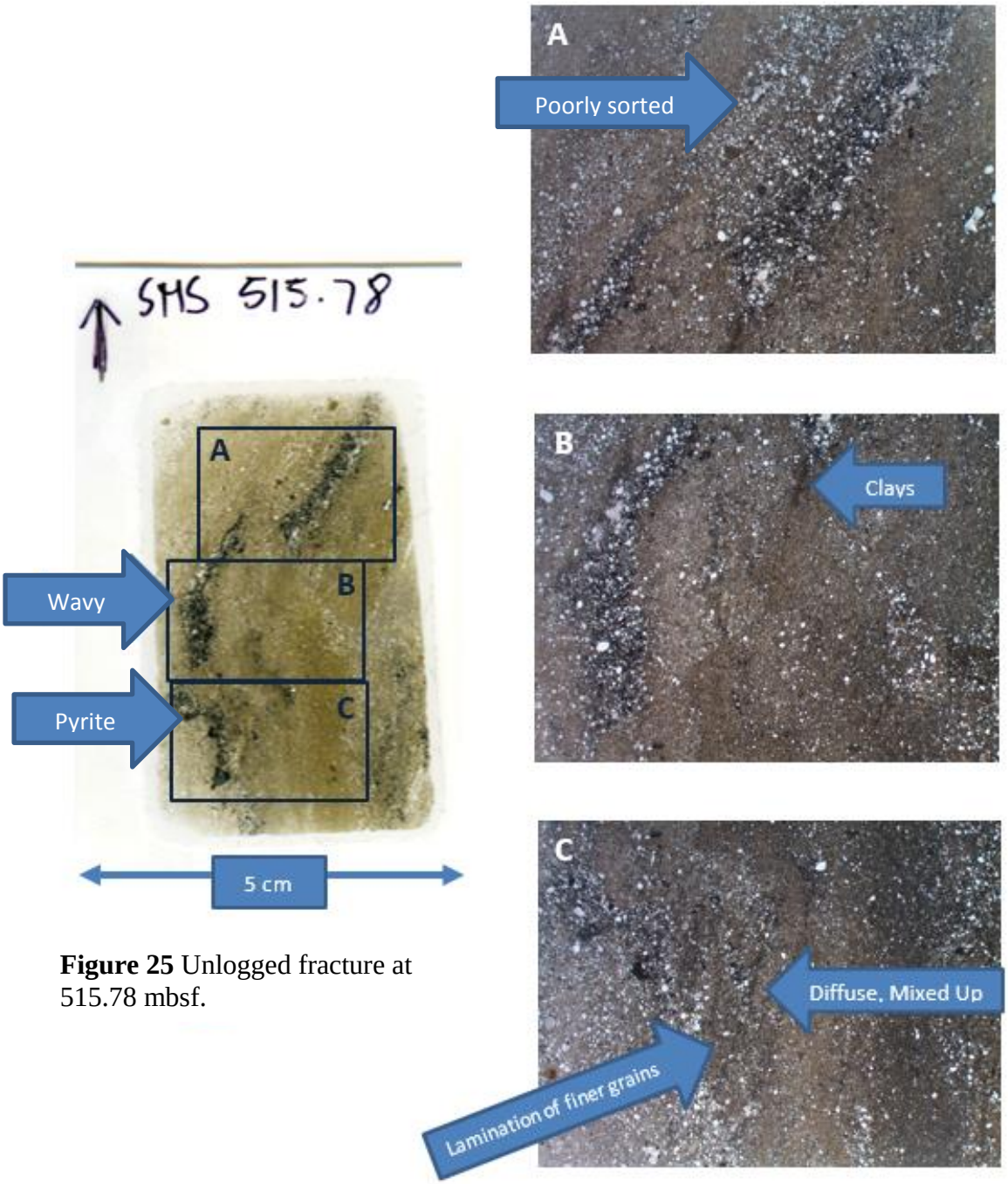


**Figure 25** Unlogged fracture at 515.78 mbsf.

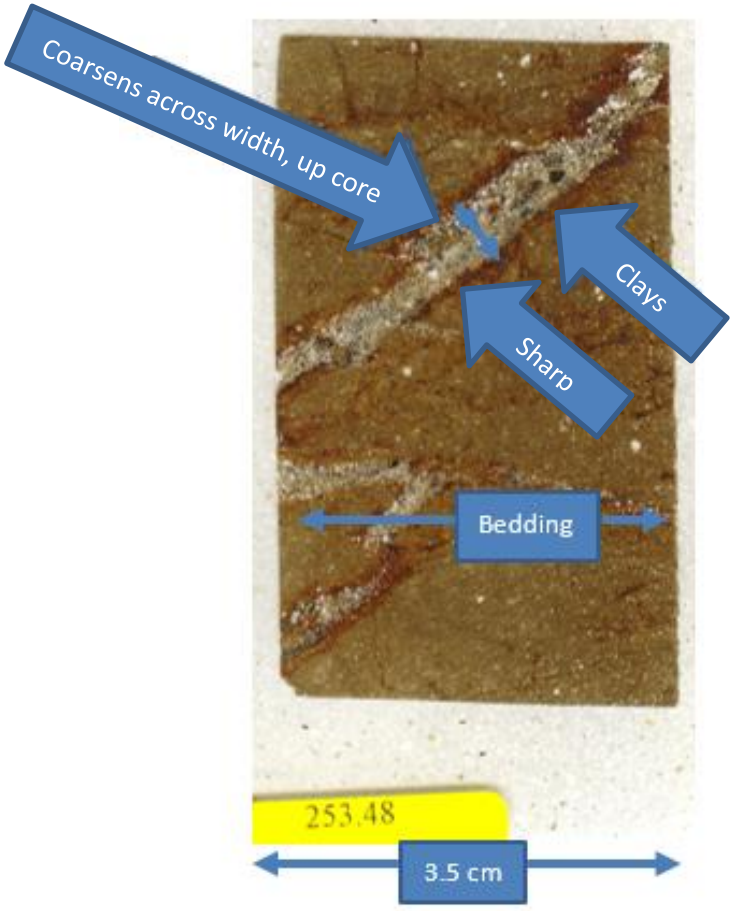


**Figure 26** Fracture 1055b at 253.48 mbsf.

| **Table 5** Other structures (+OR- 1m from CD) |
|---|
| soft sediment defm., convolute bedding, boxwork veins, flame structures, faint breccia, two CDs in thin section, local brecciation |
| flame structures, microfaulting, veins |
| conjugate fractures |
| syneresis cracks |
| boxwork veins, convolute bedding, synsedimentary microfaulting, local brecciation |
| boxwork veins, syneresis cracks |
| syneresis cracks, boxwork veins, conjugate offset |
| boxwork veins, convolute bedding, small scale fractures, pyrite in clastic fill & vise versa |
| soft sed defm., convolute bedding, boxwork veins |
| normal faults, convolute bedding, soft sed defm |
| veins, normal offset, soft sed defm |
| convolute bedding, conjugate w/ another clastic band, broken fossils, second zone of intrusion |
| more CDs, brecciation zone above dike, normal faults |

**Table 5** Other structures logged within 1 meter of CDs. Sourced from sedimentary logs compiled by Fielding et al. (2008).

### *Orientation of AND-2A Clastic Dikes*

Table 6 details observations of CD orientation made from thin section samples. CDs observed in thin section samples had dip angles ranging from 30 degrees to nearly vertical. These CDs typically formed at an angle of 30-60 degrees relative to the bedding that they cross cut. Some CDs formed at higher angles and in some cases formed perpendicular to bedding.

Stereoplots of CD attitudes of all features originally recorded as possible CDs during fracture logging by Paulsen et al. (2008) reveal two main patterns of CD geometry (Figure 27, Appendix B). CDs with relatively steep dip angles are arranged into sets, as shown in intact intervals 355.81-367.59, 367.59-374.28, and 310.56-313.86 (Figure 27). CDs with shallower dip angles have more dispersed attitudes and do not form distinct sets, for example in intact intervals 188.19-191.23, 378.38-383.31, and 296.51-301.17 (Figure 27). Some intact intervals had insufficient CD attitude data to establish meaningful orientation patterns.

A chart of dip angle vs. depth for all logged possible CDs was compiled using a 2 meter moving average to determine if CD dip angles showed any changes with depth (Figure 28). This plot shows a wide range of dip angles for CDs in AND-2A. There is no increase or decrease in dip with depth, and there is no discernable pattern of change in dip angle with depth.

A histogram of dip angle showing the number of CDs within 10 degree dip angle intervals (Figure 29) was made to determine if CD orientation was compatible with dip angle predictions for a horizontal (glacial) shearing regime or an Andersonian normal fault regime.

| **Table 6 Orientation** | | | | | |
|---|---|---|---|---|---|
| **Fracture #** | **Top Depth*** | Dip angle* | DD* | Relative to bedding | Intact Interval* |
| 400 | 89.82 | 87 | 61 | low angle | 89.32-91.3 |
| 401 | 91.45 | 63 | -126 | perpendicular | 91.3-95.1 |
| 653 | 138.65 | 0-15 | --- | parallel | 137.76-140.62 |
| Not Logged | 233.54 | * | --- | low angle | 232.65-238.16 |
| 1055b | 253.47 | 58 | 32 | low angle | 251.51-263.46 |
| 1061b | 257.99 | 88 | -73 | perpendicular | 251.51-263.46 |
| 1064b | 258.7 | 70 | 69 | high angle | 251.51-263.46 |
| 1505 | 407.42 | 70 | -170 | low angle | missing!!! |
| 1689 | 472.23 | 15-20 | --- | low angle | 471.87-476.88 |
| Not Logged | 515.79 | 70-80 | --- | perpendicular | 497.26-527.41 |
| 1840 | 533.75 | 76 | -19 | high angle | 527.41-546.35 |
| 1922 | 575.27 | 59 | -26 | low angle | 570.52-582.20 |
| 2172 | 679.01 | 34 | -74 | low angle | 666-701.68 |

**Table 6** Observations of CD orientation. *sourced from AND-2A photos and fracture logs compiled by Paulsen et al. (2008).

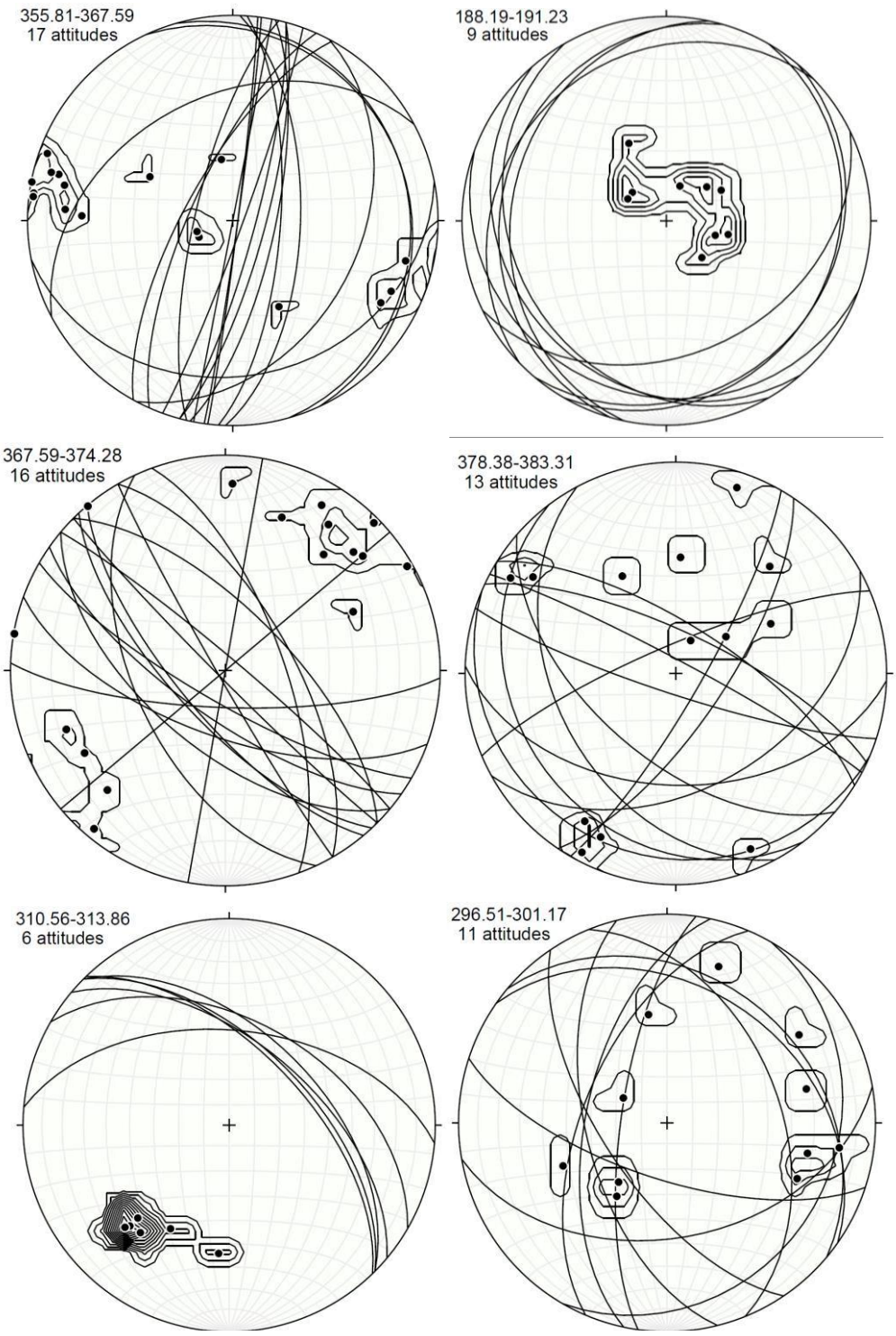


**Figure 27** Stereoplots showing two main patterns of CD geometry: steep and oriented into sets (left), as compared to shallow and not oriented into sets (right).

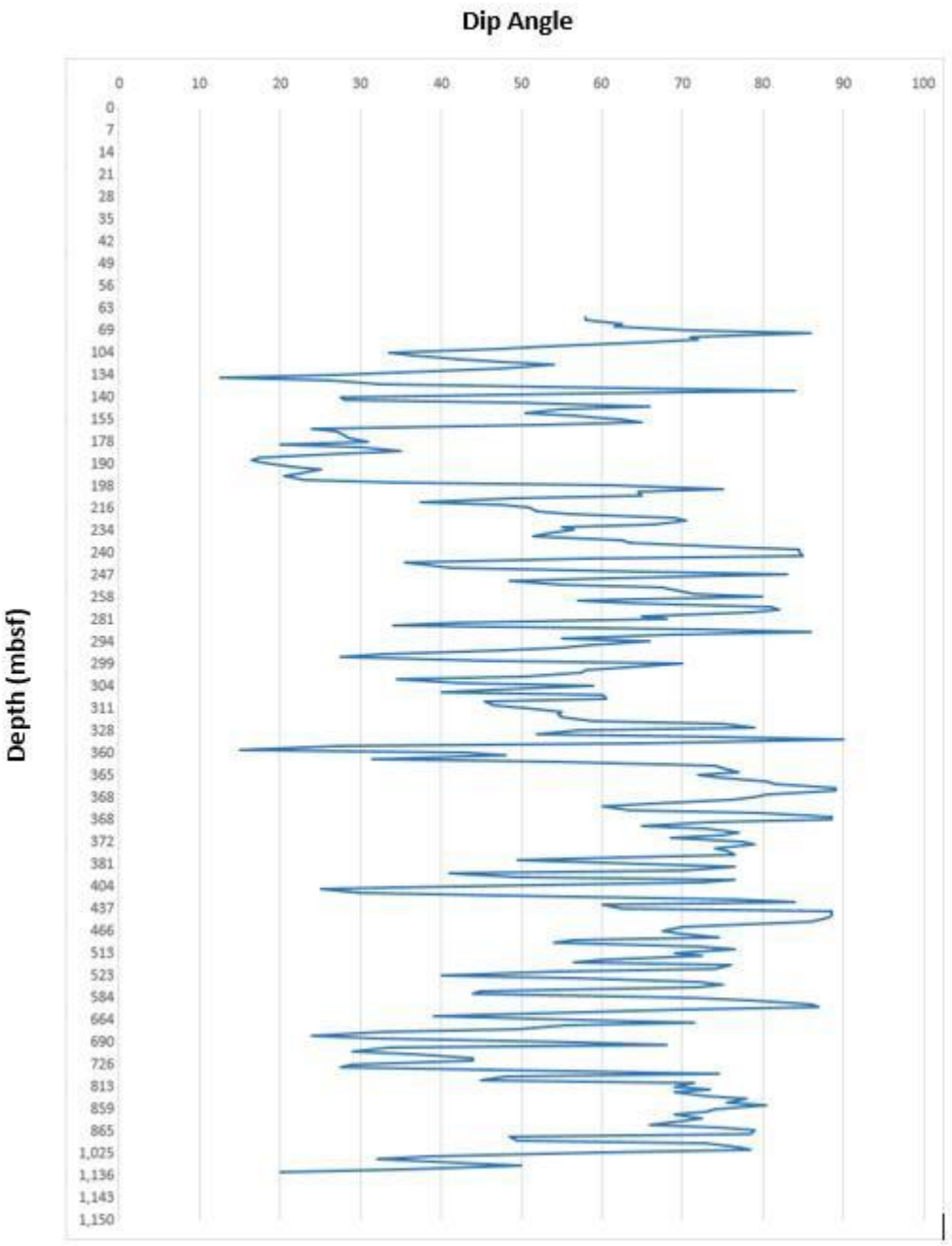


**Figure 28** CD dip vs. depth plotted using a 2 m moving average. There is no reduction of dip with depth.

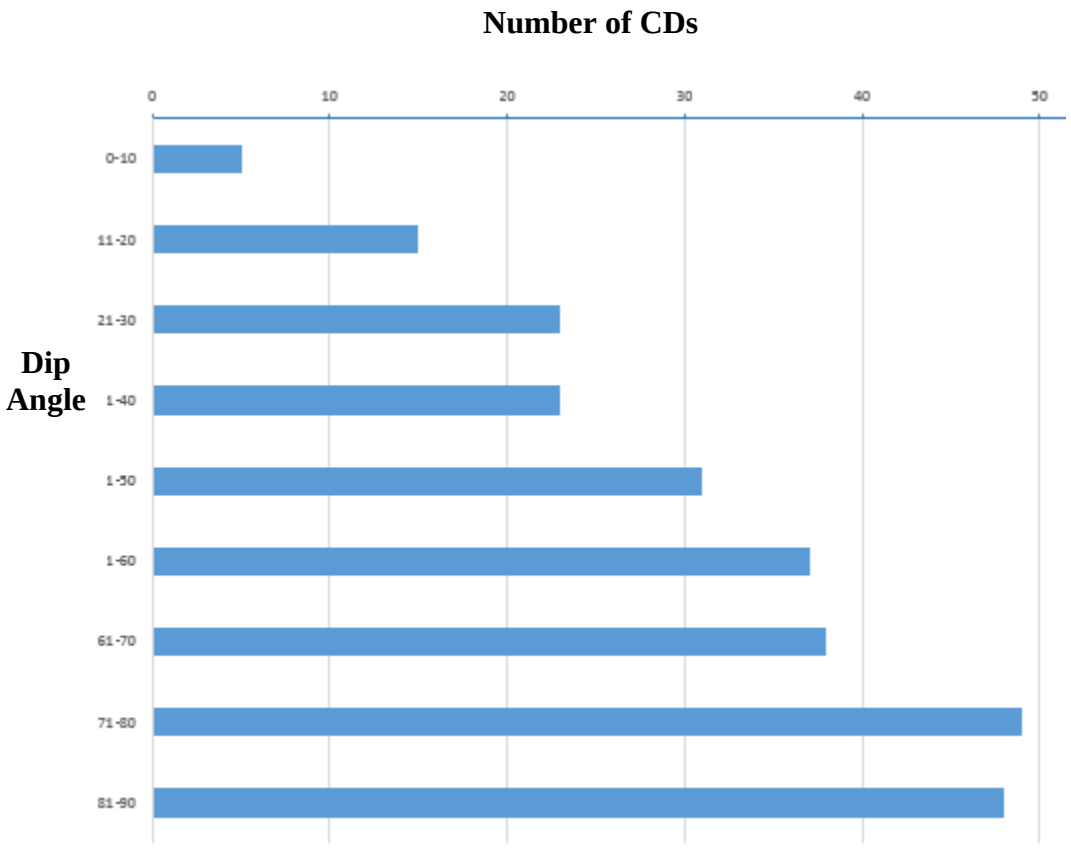


**Figure 29** Histogram plotting the number of CDs within 10 degree bins of dip angle. The majority of AND-2A CDs occur with dips of greater than 60 degrees.

### *Glacial Proximity to AND-2A Clastic Dikes*

Findings from Passchier et al. (2011) and Fielding et al. (2011), (Tables 7 and 8), show that the majority of CDs sampled for this study occur in diamictite lithology host rocks. Fewer CDs were found to occur in siltstone and sandstone lithologies. Six of the total 13 CDs occur in diamictite or conglomeratic strata interpreted to be ice proximal at the time of deposition according to the facies interpretation of Passchier et al. (2011). Five CDs occur in ice-proximal to ice-distal diamictite lithologies. Two CDs occur in siltstone facies interpreted to have been deposited as hemipelagic fallout.

According to the facies association defined by Fielding et al. (2011), four CDs occur in diamictites deposited in ice-proximal glaciomarine to subglacial environments, four CDs occur in diamictites and interlaminated sandstones interpreted to have been deposited in glaciomarine conditions affected by ice rafting. The five remaining CDs occur in siltstones deposited in open marine and restricted coastal settings.

**Table 7**

| | | Passchier et. al. (2011) | | |
|---|---|---|---|---|
| **Fracture #** | **Top Depth** | Facies | Depositional Environment | Ice Proximity |
| 400 | 89.82 | Dm | Ice-proximal glaciomarine or subglacial | |
| 401 | 91.45 | Zs | Pelagic and hemipelagic with ice rafting | |
| 653 | 138.65 | Dm | Ice-proximal glaciomarine or subglacial | |
| Not Logged | 233.54 | Ds | Ice-proximal to ice distal glaciomarine | |
| 1055b | 253.47 | Dm | Ice-proximal glaciomarine or subglacial | |
| 1061b | 257.99 | Dm | Ice-proximal glaciomarine or subglacial | |
| 1064b | 258.7 | Dm | Ice-proximal glaciomarine or subglacial | |
| 1505 | 407.42 | Ds | Ice-proximal to ice distal glaciomarine | |
| 1689 | 472.23 | Ds | Ice-proximal to ice distal glaciomarine | |
| Not Logged | 515.79 | Ds | Ice-proximal to ice distal glaciomarine | |
| 1840 | 533.75 | G | Ice-proximal glaciofluvial, ice-shelf | |
| 1922 | 575.27 | Zb | Hemipelagic with rare ice rafting | |
| 2172 | 679.01 | Ds | Ice-proximal to ice distal glaciomarine | |
| | | Passchier GSEs- 906, 763, 659, 250, 144, 60 mbsf | | |

**LEGEND**

| | | |
|---|---|---|
| | Dm | Ice-proximal glaciomarine or subglacial |
| | G | Ice-proximal glaciofluvial, ice-shelf collapse |
| | Ds | Ice-proximal to ice distal glaciomarine |
| | Zs | Pelagic and hemipelagic with ice rafting |
| | Zb | Hemipelagic with rare ice rafting |

**Table 8**

**Fielding et. al. (2011)**

| Motif | Sequence | Facies # | Depositional Environment | Ice Proximity |
|---|---|---|---|---|
| 1 | 70 | 8 | Ice-proximal glaciomarine to subglacial | |
| 1 | 69 | 3 | Open marine to restricted coastal settings | |
| 4a | 67 | 8 | Ice-proximal glaciomarine to subglacial | |
| 1 | 61 | 4 | Open marine shoreface to upper offshore | |
| 1 | 60 | 4 | Open marine shoreface to upper offshore | |
| 1 | 60 | 6 | Open glaciomarine | |
| 1 | 60 | 8 | Ice-proximal glaciomarine to subglacial | |
| 3 | 50 | 7 | Open, proximal glaciomarine conditions | |
| 3 | 43 | 5 | Open marine conditions | |
| 3 | 41 | 7 | Open, proximal glaciomarine conditions | |
| 3 | 39 | 8 | Ice-proximal glaciomarine to subglacial | |
| 3 | 34 | 3 | Open marine to restricted coastal settings | |
| 2 | 31 | 7 | Open, proximal glaciomarine conditions | |

**LEGEND**

| | | |
|---|---|---|
| | 8 | Ice proximal glaciomarine to subglacial |
| | 7 | Open, proximal glaciomarine conditions |
| | 6 | Open glaciomarine, ice rafting |
| | 5 | Open marine conditions, 10-60m, minor ice rafting |
| | 4 | Open marine shoreface to upper offshore, 10-40m, minor ice rafting |
| | 3 | Open marine to restricted coastal settings, 10-80m, minor ice rafting |

# Discussion

Through petrographic observation of variations in CD morphology, intrusive material, internal textures, and host rocks, this study constrains the types of processes that led to the formation of CDs in the AND-2A rock core, as the observation of soft sediment deformation structures has the potential to provide direct insight into the specific conditions that existed at the time of formation (Mills, 1983). Stereoplots of CD attitudes and histograms of CD dip angle data paired with ice proximity analysis allows for the interpretation of CDs as markers of either glacial or tectonic history.

## *Processes involved with Clastic Dike Injection in AND-2A*

Table 9 details CD attributes observed in this study and provides an explanation of what these attributes may indicate about the formation of CDs in AND-2A (after Hurst et al., 2011).

Eight AND-2A CDs show planar dike geometry (Table 1), which indicates that the formation of these opening-mode fractures in AND-2A was driven by high fluid pressures in relatively cohesive sediments (Hurst et al., 2011). This also indicates that there were pre-existing planes of weakness in the sediments of AND-2A, which opened and filled with sediments as they experienced favorable stress directions. Five CDs in AND-2A occur with wavy and increasingly complex dike geometries (Table 1), indicating that the original host rock fabric was anisotropic prior to injection of these CDs (Hurst et al., 2011).

Seven CDs in AND-2A show distinctively sharp margins (Table 1), indicating abrasive, erosive flow of sand during injection. Sharp margins observed in AND-2A also

indicate that fractures could have formed prior to the development of high fluid pressures, and were then propped open with clastic material as the stress regime allowed (Hurst et al., 2011). Four CDs in AND-2A occur with diffuse margins (Table 1), indicating that the host rock was not necessarily fractured during the movement of clastic material, and that more complex processes of injection occurred (Hurst et al., 2011). CDs with diffuse margins are difficult to describe in terms of fracture systems (Hurst et al., 2011). The high number of CDs having sharp margins in AND-2A indicates that many CDs in AND-2A were formed as primary natural hydraulic fractures or by injecting into a previously existing fracture that was favorably oriented to the stresses at the time of injection.

Grain size of AND-2A CD intrusive material (Table 2) provides a direct indicator of the relative amounts of energy needed to transport material (Hurst et al., 2011). CDs having intrusive material with very coarse sand and larger grain sizes require more energy to be transported as compared to the finer grain sizes (Hurst et al., 2011). Two CDs in AND-2A have an average grain size of silt while three AND-2A CDs have an average grain size of very fine sand, which indicate that the sediments filling these CDs did not require very much energy to be transported. Four CDs show an average grain size of fine sand and four CDs in AND-2A have an average grain size of medium sand, indicating that the sediments filling these CDs required more energy to be transported. The range in average grain size of CD intrusive material observed in AND-2A indicates that water velocities supporting clastic injection varied during the formation of these CDs.

Grain sorting within AND-2A CDs (Table 3) provides a signature of the transport mechanism responsible for particle movement (Hurst et al., 2011). Four CDs in AND-2A have very well sorted intrusive material, two CDs are well sorted, and five CDs are moderately

sorted. Very well to moderate sorting of CD intrusive material in AND-2A indicates that coarser grains were deposited within CD margins as finer grains were flushed out by high injection velocities (Hurst et al., 2011). Two CDs in AND-2A are poorly sorted, which indicates that fluidized sand material was very clast-rich, and as a result hindered the sorting mechanisms that occurred in other AND- 2A CDs (Hurst et al., 2011).

Two CDs in AND-2A have angular grains and six CDs show subangular grains (Table 3). Five CDs in AND-2A have subrounded grains (Table 3). During injection, fluidized material travels a relatively short distance. Therefore, variation in grain shape is almost certainly related to transport processes that occurred prior to deposition, and should not be considered to be affected by dike injection.

Grading within AND-2A CD margins (Table 3) is indicative of the sorting of clasts during the injection of sedimentary material (Hurst et al., 2011). Five CDs in AND-2A are observed with normal grading, where the coarsest grains are adjacent to CD walls, which is indicative of a turbulent flow regime (Hurst et al., 2011). Reverse grading, the coarsest grains occur in the center of the dike, is observed in five AND-2A CDs, and is indicative of laminar flow during injection (Hurst et al., 2011). Three AND-2A CDs were completely devoid of grading which is indicative of dikes whose fluidized material did not have a large grain size distribution to start with (Hurst et al., 2011). The equal distribution of normal and reverse grading of CDs suggests that both turbulent and laminar flow commonly occurred during the formation of CDs in AND- 2A.

Eight AND-2A CDs show lamination inside their margins (Table 3), which indicates variations in the velocity or viscosity of sand-charged fluids during clastic injection, or that

multiple episodes of injection may have caused the formation of AND-2A CDs (Hurst et al., 2011). Five CDs in AND-2A are devoid of lamination, indicating little variation in the flow parameters of sand- charged fluids during injection and that there was only one episode of injection.

Eight AND-2A CDs have slight to definite alignment of grains and clay particles parallel to dike margins (Table 3), which indicates the upward injection of fluid and sand in AND-2A strata (Hurst et al., 2011). The absence of alignment in some AND-2A CDs indicates that they may have been injected downwards.

The majority of AND-2A CDs examined in this study occur in diamictite lithologies (Table 4). The occurrence of clastic dikes is common in host strata that are cohesive, fine grained, and which constitute impermeable seal lithologies (Hurst et al., 2011). The fine-grained silty matrix of AND-2A diamictite lithologies allowed them to act as seals that maintained high pore fluid pressures that are required for the hydraulic injection of clastic material.

**Table 9**

| **Attribute** | **Indicator of:** |
|---|---|
| Compiled from Hurst et al. (2011). | |
| Dip angle/direction | • Relationship to regional tectonics, other structures in core, and/or subglacial shear deformation |
| Arrangement in sets | • Tensile fracture, high differential stress |
| Randomly oriented | • Low stress differential<br>• Anisotropy of sediments when formed |
| Grain size of intrusive material | • Energy needed to transport material<br>• Match with source beds |
| Grain shape of intrusive material | • Distance of transport<br>• Particle attrition during flow |
| Grain sorting | • Transport mechanism<br>• Flow regime |
| Planar dike geometry | • sand injected along planar fracture<br>• Wavy & steps: original anisotropy and/ or post injection deformation |
| Wavy & stepped geometry | • original anisotropy<br>• post injection folding/boudinage |
| Margin geometry- sharp, diffuse, etc. | • Abrasive flow of sand during injection<br>• Sediment filled fractures |
| Grading within intrusion | • Sorting of clasts during injection |
| Normal- coarsest adj. to dike walls | • Turbulent flow |
| Reverse- coarsest in center of dike walls | • Laminar Flow |
| Along length | • Typically finning upward, loss of energy |
| Grain alignment parallel to margin | • Typical of upward injection of sand<br>• Flow regime<br>• Hydroplastic shear |
| Lamination | • Multiple episodes of injection<br>• Rate of opening of fractures<br>• Variations in velocity/viscosity of sand-charged fluids |

### *Clastic Dike Injection in AND-2A: Glacial vs. Tectonic Deformation*

Figure 30 details the range of stress states that affect sediments prior to and after lithification. According to Cosgrove (1995), an isotropic stress state with a low differential stress leads to unoriented fractures, as is the case in hydrostatic or lithostatic stress states (case IV in Figure 30). In contrast, an anisotropic stress state with a high differential stress, such as is the case in a tectonic stress regime, leads to fractures that are oriented into sets (case I in Figure 30).

The presence of oriented sets of steeply-dipping CDs in AND-2A indicates the formation of CDs in a stress state with sufficient differential stress to control resulting fracture geometries. Shallowly dipping AND-2A CDs are not oriented into sets, and are markers of an isotropic stress state, in which there are low amounts of differential stress. These contrasting patterns of CD geometry in AND-2A suggest that either differential stress was not very high, and local anisotropies in host rocks caused deviation in CD orientation, or that the differing mechanical properties of lithologies present in AND-2A responded to stress by fracturing in different geometries. Stereoplot 355.81-367.59 (Figure 31), which shows both types of geometries within the same intact interval, is largely composed of a single diamictite lithology (Fielding et al., 2008). This indicates that in this intact interval of AND-2A, local differences in the host rock, as opposed to different mechanical properties of sedimentary layers, caused the formation of the contrasting orientation patterns observed in AND-2A CDs.

Structures forming early in the development of sedimentary basins are typically compacted as the basin strata dewaters. As a result, these structures may experience an overall reduction of dip angle with depth (Davison, 1987). The histogram of CD dip angle vs. depth

for CDs logged in the AND-2A core (Figure 28) does not show any pattern of change in dip angle with depth. The absence of a dip angle reduction with depth in the dip angles of CDs in AND-2A indicates that they did not experience any vertical shortening. CDs in AND-2A likely formed after a large amount of sedimentary compaction in the VLB had already taken place. The absence of folded CDs and other structures related to vertical shortening corroborates this interpretation.

In a horizontal glacial shearing model, low-angle dips (<45 degrees) are common, while in an Andersonian model, conjugate normal faults and vertical extension fractures (>60 degrees) occur with the most frequency. A histogram of CD dip angle (Figure 29) shows that less than 7% of CDs observed in AND-2A have dips of less than 20 degrees, while more than 50% of AND-2A CDs have dips ranging from 60-90 degrees. The high occurrence of CDs with dips of >60 degrees suggests that CDs in AND-2A formed as the result of an Andersonian normal fault regime with a vertical maximum compressive principal stress direction.

Table 10 summarizes grounded ice sheet proximity to the host rock strata in which AND-2A CDs occur. Six AND-2A CDs occur in diamictite or conglomeratic strata which are interpreted to have been ice proximal at the time of deposition according to the facies divisions of Passchier et al. (2011). Five AND-2A CDs occur in ice-proximal to ice-distal diamictite lithologies. Two AND-2A CDs occur in siltstone facies interpreted to have been deposited as hemipelagic fallout. Four AND-2A CDs occur within 10 meters of an interpreted glacial surface of erosion. According to the facies association defined by Fielding et al. (2011), four AND-2A CDs occur in diamictites deposited in ice-proximal glaciomarine to subglacial environments, and four AND-2A CDs occur in diamictites and interlaminated

sandstones interpreted to have been deposited in glaciomarine conditions affected by ice rafting. Five remaining AND-2A CDs occur in siltstones deposited in open marine and restricted coastal settings. The observed spatial distribution of CDs in ice proximal to ice distal depositional environments, shown in Tables 7 and 8, indicates that deformation of the substrate beneath a grounded ice sheet is likely not the mechanism for CD injection, suggesting their formation may be controlled by tectonic activity.

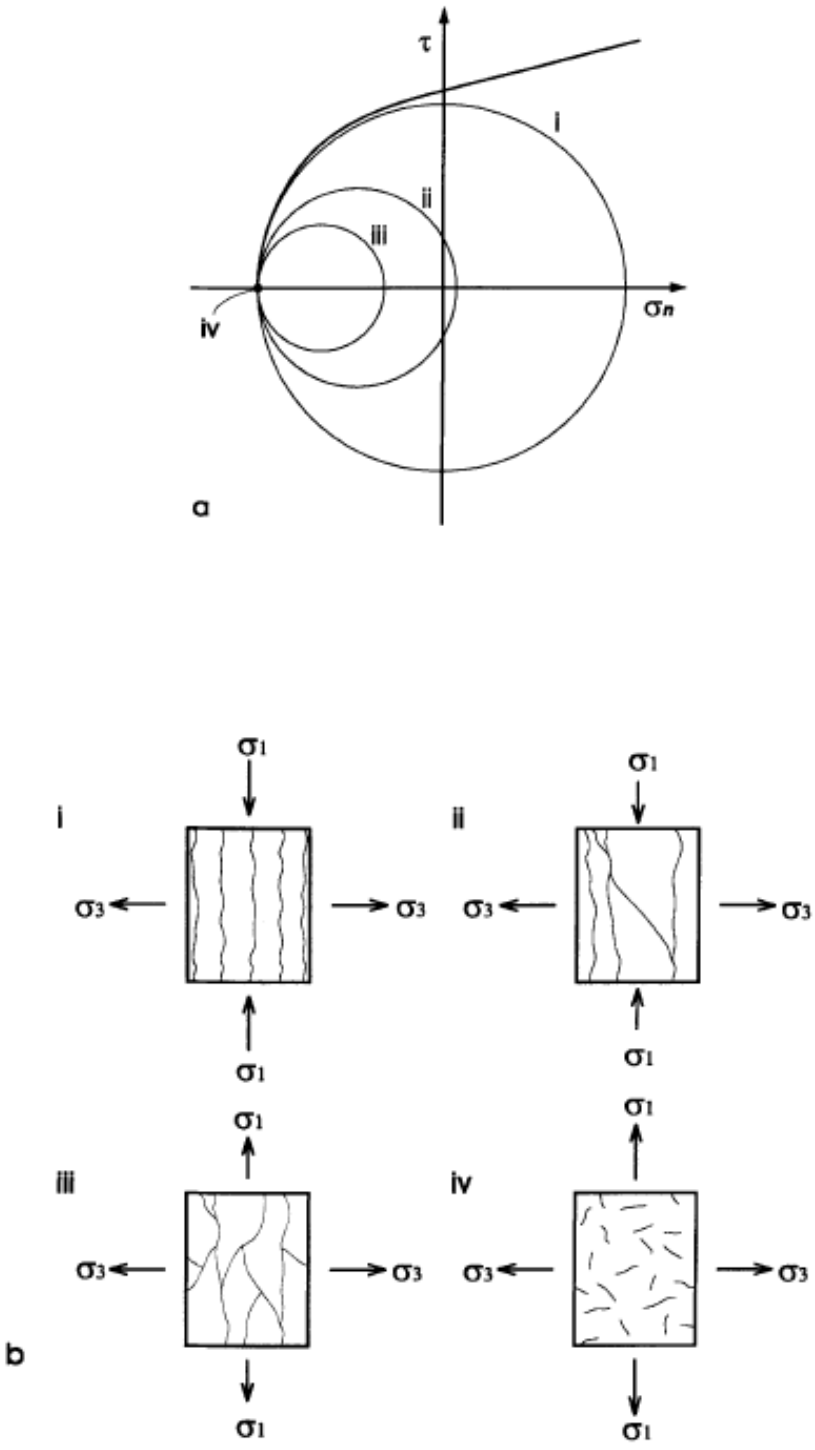


**Figure 30** Four different stress states that can lead to tensile failure. (I) a high differential stress leads to oriented fractures, (II) and (III) progressively lower differential stresses lead to fractures with less preferred orientation, and (IV) an isotropic stress state leading to unoriented fractures (Cosgrove, 1995).

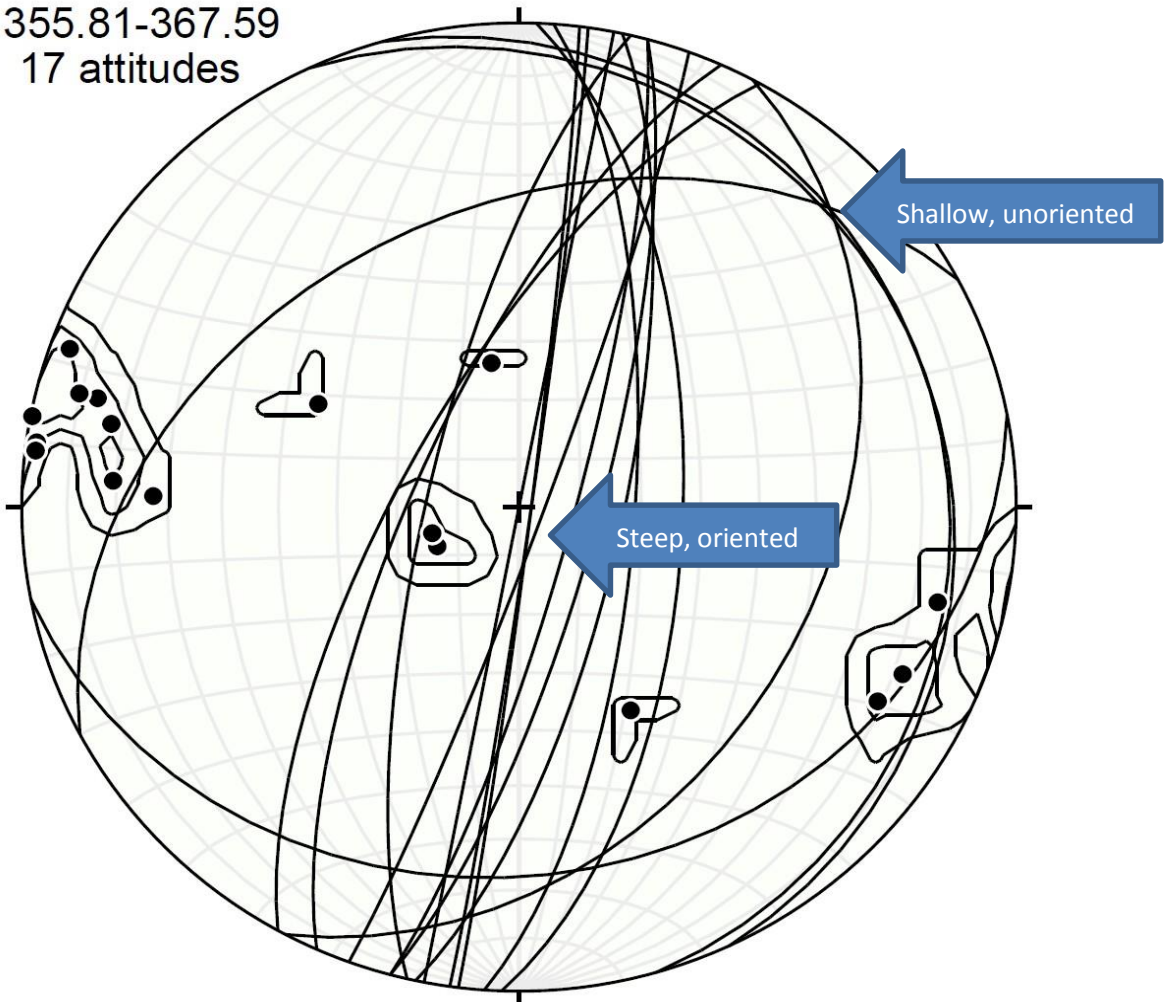


**Figure 31** Shows stereoplot of intact interval 355.81-367.59, with steeply dipping oriented CDs and shallowly dipping unoriented CDs in AND-2A. This interval is largely composed of diamictite (Fielding et al., 2008).

**Table 10**

| Fracture # | Top Depth | Ice Proximity | Ice Proximity |
|---|---|---|---|
| 400 | 89.82 | | |
| 401 | 91.45 | | |
| 653 | 138.65 | | |
| Not Logged | 233.54 | | |
| 1055b | 253.47 | | |
| 1061b | 257.99 | | |
| 1064b | 258.7 | | |
| 1505 | 407.42 | | |
| 1689 | 472.23 | | |
| Not Logged | 515.79 | | |
| 1840 | 533.75 | | |
| 1922 | 575.27 | | |
| 2172 | 679.01 | | |

| | |
|---|---|
| | Ice-proximal glaciomarine or subglacial |
| | Ice-proximal glaciofluvial, ice-shelf collapse |
| | Ice-proximal to ice distal glaciomarine |
| | Pelagic and hemipelagic with ice rafting |
| | Hemipelagic with rare ice rafting |

| | |
|---|---|
| | Ice proximal glaciomarine to subglacial |
| | Open, proximal glaciomarine conditions |
| | Open glaciomarine, ice rafting |
| | Open marine conditions, 10-60m, minor ice rafting |
| | Open marine shoreface to upper offshore, 10-40m, minor ice rafting |
| | Open marine to restricted coastal settings, 10-80m, minor ice rafting |

## Conclusions

The AND-2A rock core sedimentary succession provides an unprecedented understanding of tectonic, glacial, and climatic processes at work in Antarctica (Florindo et al., 2008). This study examined CDs occurring in the AND-2A core in order to determine the drivers of their formation in the Antarctic glaciated rift environment. CDs, a result of natural hydraulic fracturing, most commonly form as a result of overpressure associated with tectonic activity (Jolly and Lonergan, 2002). Despite recognition of their importance in the evolution of sedimentary basins, the processes leading to their formation remain poorly understood (Huuse et al., 2010). Through the observation of CD morphology, intrusive material, texture, host rock, orientation, and the sedimentary facies in which they formed, this study sought to determine the processes responsible for the formation of CDs observed in the AND-2A sedimentary rock core, and to determine whether CDs were markers of Antarctica's tectonic history, glacial history, or both.

The AND-2A CD attributes established by petrographic observations of 13 thin section samples are interpreted here in light of the process-oriented overview of clastic intrusion processes and attributes by Hurst et al. (2011) (Table 9). The formation of planar opening-mode CD fractures in AND-2A was caused by high fluid pressures in relatively cohesive sediments. Local anisotropies in the host rock fabric led to the formation of wavy CD fractures. A large number of CDs occur with sharp margins in AND-2A, indicating that the sediments experienced the erosive flow of sand during injection, and that previously existing fractures which were favorably oriented to the stresses at the time reopened and filled with clastic material. Grain size variation within CD margins indicates that water velocities during injection varied during the formation of CDs in AND-2A. Most AND-2A

CDs are moderately to well sorted, indicating that finer grains were flushed out during injection by high fluid velocities. A few AND-2A CDs are poorly sorted, indicating that the original fluidized material was very clast rich, hindering sorting mechanisms. The presence of subangular to angular grains within CD margins mark transport processes that occurred prior to deposition. Normal and reverse grading are present within AND-2A CDs, suggesting that they formed in both turbulent and laminar flow regimes. Lamination within the margins of AND-2A CDs indicates that there were variations in the flow parameters of sand-charged fluids during injection, or that there were multiple episodes of injection. The alignment of grains parallel to dike margins in AND-2A CDs indicates that fluids were injected upwards into overlying strata. The fine-grained silty matrix of AND-2A diamictite lithologies prevented fluid flow and contributed to the maintenance of high pore fluid pressures, which resulted in clastic injection.

The orientation of CD fractures is controlled by the stresses affecting the host strata at the time of CD formation. Stereoplots revealed two main patterns of CD geometry (Figure 27), steep and oriented into sets, contrasted with shallow and unoriented. Fractures oriented into sets are interpreted to have developed in sediments experiencing a differential stress, while unoriented fractures formed in regimes with an isotropic stress state (Figure 30). These patterns suggest that an anisotropic stress state controlled the formation of steep sets of CDs in AND-2A, while local variations in the host rock caused the development of shallowly-dipping unoriented sets. CDs in AND-2A do not have an overall reduction of dip with depth and, therefore, formed after significant compaction of host sediments had already occurred in the VLB. The majority of CD dip values are greater than 60 degrees, suggesting AND-2A CDs formed in a stress regime with the maximum stress oriented vertically, as opposed to one of

horizontal shearing related to deformation of the substrate by over-riding grounded ice sheets.

Interpretations of glacial proximity to CD host strata from Passchier et al. (2011) and Fielding et al. (2011) show that AND-2A CDs formed in strata deposited in both ice-proximal and ice-distal environments. The occurrence of CDs in AND-2A therefore does not show a consistent spatial relationship with ice-proximity. This result, together with the CD orientations, suggest that deformation beneath grounded ice was not responsible for CD formation. Instead, overpressures, possibly associated with the overburden of ice in the region, probably played a pivotal role in the formation of CDs observed in the AND-2A sedimentary rock core. The orientation of CDs into steeply-dipping sets, consistent with an Andersonian normal fault regime, suggests that AND-2A CDs formed in association with tectonic activity.

## Suggestions for Future Research

The injection of CDs involves the formation of a sediment-water mixture, but the behavior of this mixture during the movement of clastic material is poorly constrained due to the lack of information on parameters needed to describe complex fluid dynamics (Huuse et al., 2010). Huuse et al. (2010) cite the need for a better understanding of the spatio-temporal occurrence of fluid flow phenomena to determine the timing of clastic intrusions in the process of diagenesis and the development of sedimentary basins, and stated that this understanding may be provided by the observation of outcrop examples, sampling of active fluid flow systems, and numerical basin modelling. Van der Meer et al. (2009) similarly suggested that an understanding of the relationship between clastic dikes and glacial sediments would be aided by experiments to determine the exact timing of their formation and the spatial relationship between the site of formation and glacier extent.

Petrographic analysis of thin section samples of the AND-2A sedimentary rock core in this study was limited to 13 samples. Analysis of additional CD samples will provide a more complete understanding of CD occurrence within the context of the AND-2A sedimentary rock core. This will allow for more extensive characterization of their physical properties, and thereby will contribute to a better understanding of the processes leading to their formation.

This study aggregated orientation data so that anything logged as a CD was incorporated, even if there was some uncertainty in the diagnostic value of this interpretation. For example, CDs could be logged with a “CD” or a “CD?”, or even may be logged as something like “F?V?CD?” (e.g., this fracture could be a fault, vein, or CD). Further analysis of the orientation of CDs in the AND-2A core will require a diagnostic method to determine

which fractures logged as CDs hold up to their initial characterization. An understanding of which fractures can be considered CDs will allow for greater credibility in orientation analysis. In addition, an expanded glacial proximity table could be compiled. Inclusion of more CDs in this analysis would provide a larger scale context of their occurrence.

The Coulman High Project is the next experiment proposed by the ANDRILL project, and will provide another high-quality sedimentary succession from the Paleogene into the Lower Miocene. This rock core will enhance understanding of the tectonic history of West Antarctica, and how Antarctic ice sheets responded to high levels of $CO_2$. This core will provide a host of new structures, likely including clastic intrusions, to be studied and characterized.

## References Cited

Cosgrove, J.W. (1995). The expression of hydraulic fracturing in rocks and sediments. *Geological Society Special Publication.* 92, pp. 187-196.

Cosgrove, J. W. (2001). Hydraulic fracturing during the formation and deformation of a basin: A factor in the dewatering of low-permeability sediments. *AAPG Bulletin.* 85 (4), pp. 737-748.

Davison, I. (1987). Normal fault geometry related to sediment compaction and burial. *Journal of Structural Geology.* 9 (4), pp. 393-401.

Dixon, R.J., Schofield, K., Anderton, R., Reynolds, A.D., Alexander R.W.S., Williams, M.C., Davies, K.G. (1995). Sandstone diapirism and clastic intrusion in the Tertiary submarine fans of the Bruce-Beryl Embayment, Quadrant 9, UKCS. *Geological Society, London, Special Publications.* 94, pp. 77-94.

Fielding, C., Atkins, C.B., Bassett, K.N., Browne, G.H., Dunbar, G.B., Field, B.D., Frank, T.D., Krissek, L.A., Panter, K.S., Passchier, S., Pekar, S.F., Sandroni, S., Talarico, F., ANDRILL-SMS Science Team. (2008). Sedimentology and Stratigraphy of the AND-2A Core, ANDRILL, Southern McMurdo Sound Project, Antarctica. *Terra Antarctica.* 15 (1), pp. 77-112.

Fielding, C., Browne, G., Field, B., Florindo, F., Harwood, D.M. (2011). Sequence stratigraphy of the ANDRILL AND-2A drillcore, Antarctica: A long-term, ice-proximal record of Early to Mid-Miocene climate, seal-level, and glacial dynamism. ANDRILL Research and Publications. 43.

Fitzgerald, P. (2002). Tectonics and landscape evolution of the Antarctic plate since the breakup of Gondwana, with emphasis on the West Antarctic Rift System and the Transantarctic Mountains. *Royal Society of New Zealand Bulletin.* 35, pp 453-469

Florindo, F., Harwood D.M., Talarico, F., Levy, R.H., ANDRILL-SMS Science Team (2008). Background to the ANDRILL Southern McMurdo Sound Project, Antarctica. *Terra Antarctica.* 15 (1), pp. 13-20.

Hillier, R.D., Cosgrove, J.W. (2002). Core and seismic observation of overpressure-related deformation within Eocene sediments of the Outer Moray Firth, UKCS. *Petroleum Geoscience.* 8, pp. 141-149.

Hurst, A., Scott, A., Vigorito, M. (2011). Physical characteristics of sand injectites. *Earth Science Reviews.* 106, pp. 215-246.

Huuse, M., Jackson, C.A., Van Rensbergen, P.V, Davies, R.J., Flemings, P.B., Dixon, R.J. (2010). Subsurface sediment remobilization and fluid flow in sedimentary basins: an overview. *Basin Research.* 22, pp. 342-360.

Jolly, R.J.H., Lonergan, L. (2002). Mechanisms and controls on the formation of sand intrusions. *Journal of the Geological Society, London.* 159, pp. 605-617.

Le Heron, D.P., Etienne, J. L. (2005). A complex subglacial clastic dyke swarm, Solheimajokull, southern Iceland. *Sedimentary Geology.* 181. pp. 25-37.

Mills P.C. (1983). Genesis and diagnostic value of soft-sediment deformation structures- a review. *Sedimentary Geology.* 35. pp. 83-104.

Owen, G. (1987). Deformation processes in unconsolidated sands. *Geological Society Special Publication.* 29, pp. 11-24.

Owen, G., Massimo, M. (2011). Identifying triggers for liquefaction-induced soft-sediment deformation in sands. *Sedimentary Geology.* 235, pp. 141-147.

Owen, G., Massimo, M., Alfaro, P. (2011). Recognising triggers for soft-sediment deformation: Current understanding and future directions. *Sedimentary Geology.* 235, pp. 133-140.

Passchier, S., Browne, G., Field, B., Fielding, C.R., Krissek, L.A., Panter, K., Pekar, S.F., ANDRILL-SMS Science Team (2011). Early and middle Miocene Antarctic glacial history from the sedimentary facies distribution in the AND-2A drill hole, Ross Sea, Antarctica. *GSA Bulletin.* 123 (11/12), pp. 2352-2365.

Paulsen, T., Millan, C., Pierdominici, S., Wilson, T., Drew, S., ANDRILL-SMS Science Team (2008). Fracture logging of the AND-2A Core, ANDRILL Southern McMurdo Sound Project, Antarctica. *Terra Antarctica.* 15 (1), pp. 69-76.

Paulsen, T., Wilson, G.S. (1998). Orientation of the CRP-1 core. *Terra Antarctica.* 5 (3), pp. 319-325.

van der Meer, J.J.M., Kjaer, K.H., Kruger, J., Rabassa, J., Kilfeather, A.A. (2009). Under pressure: clastic dykes in glacial settings. *Quaternary Science Reviews.* 28, pp. 708-720

## Appendix A: Photo Examples






F# 401

91.44 mbsf

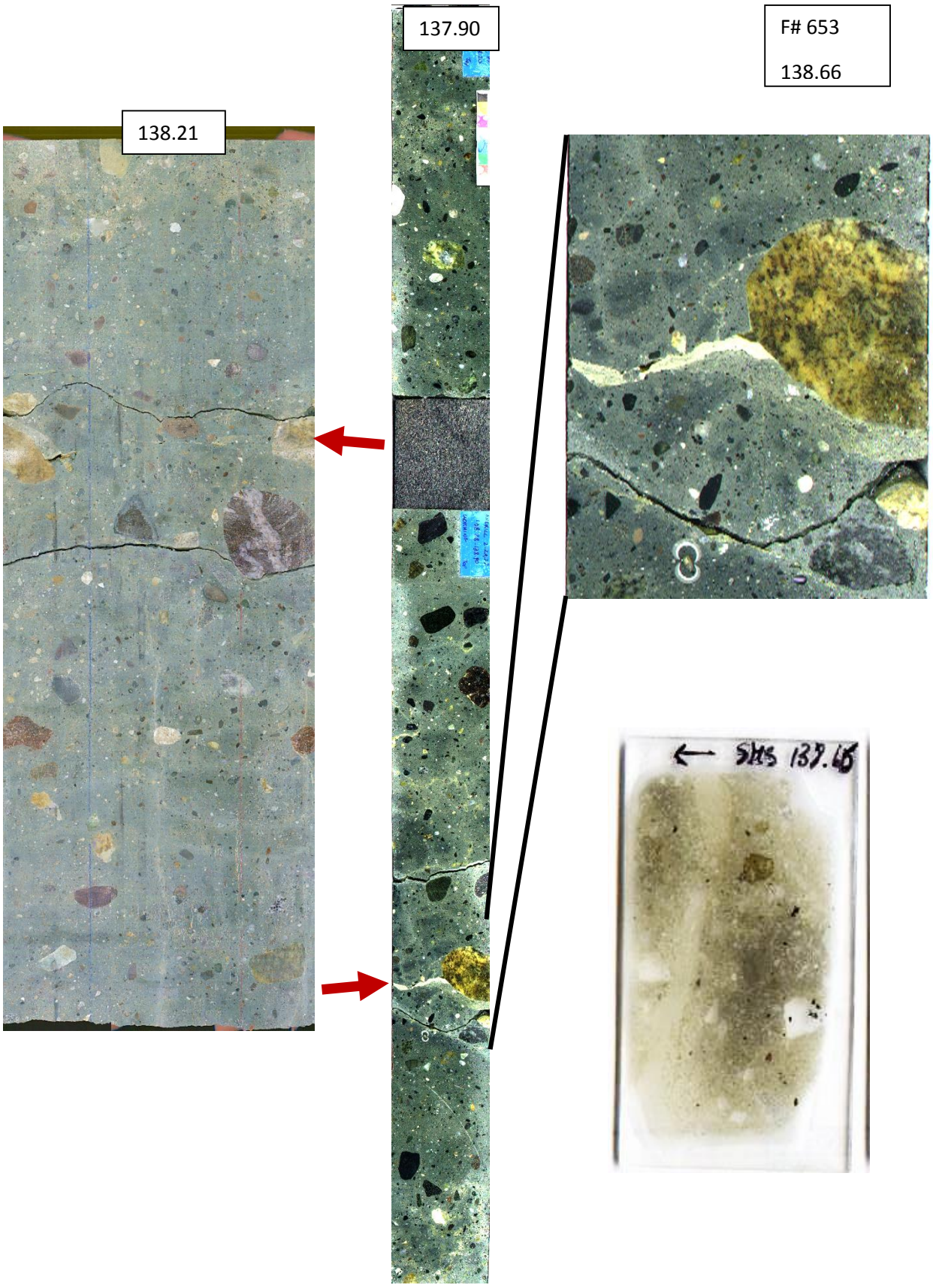
137.90
F# 653
138.66
138.21
← SMS 137.45

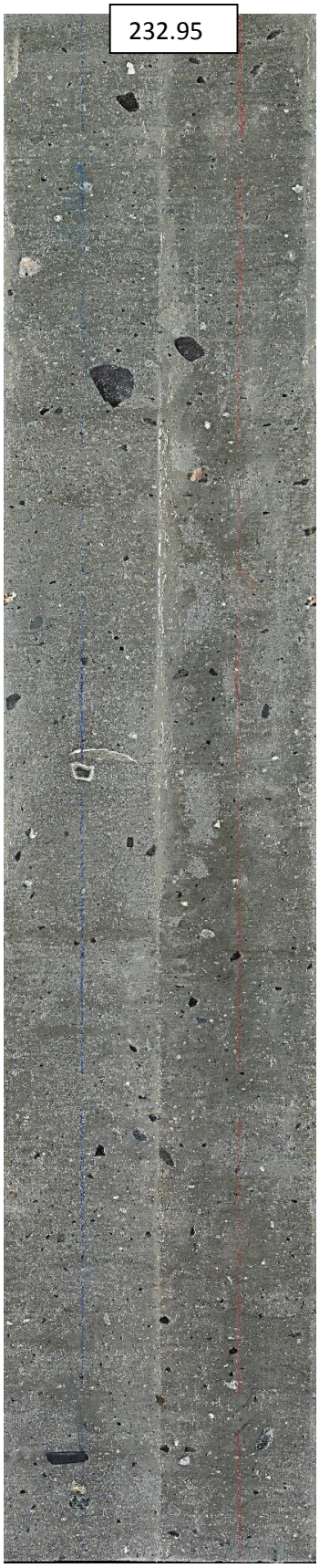
232.95

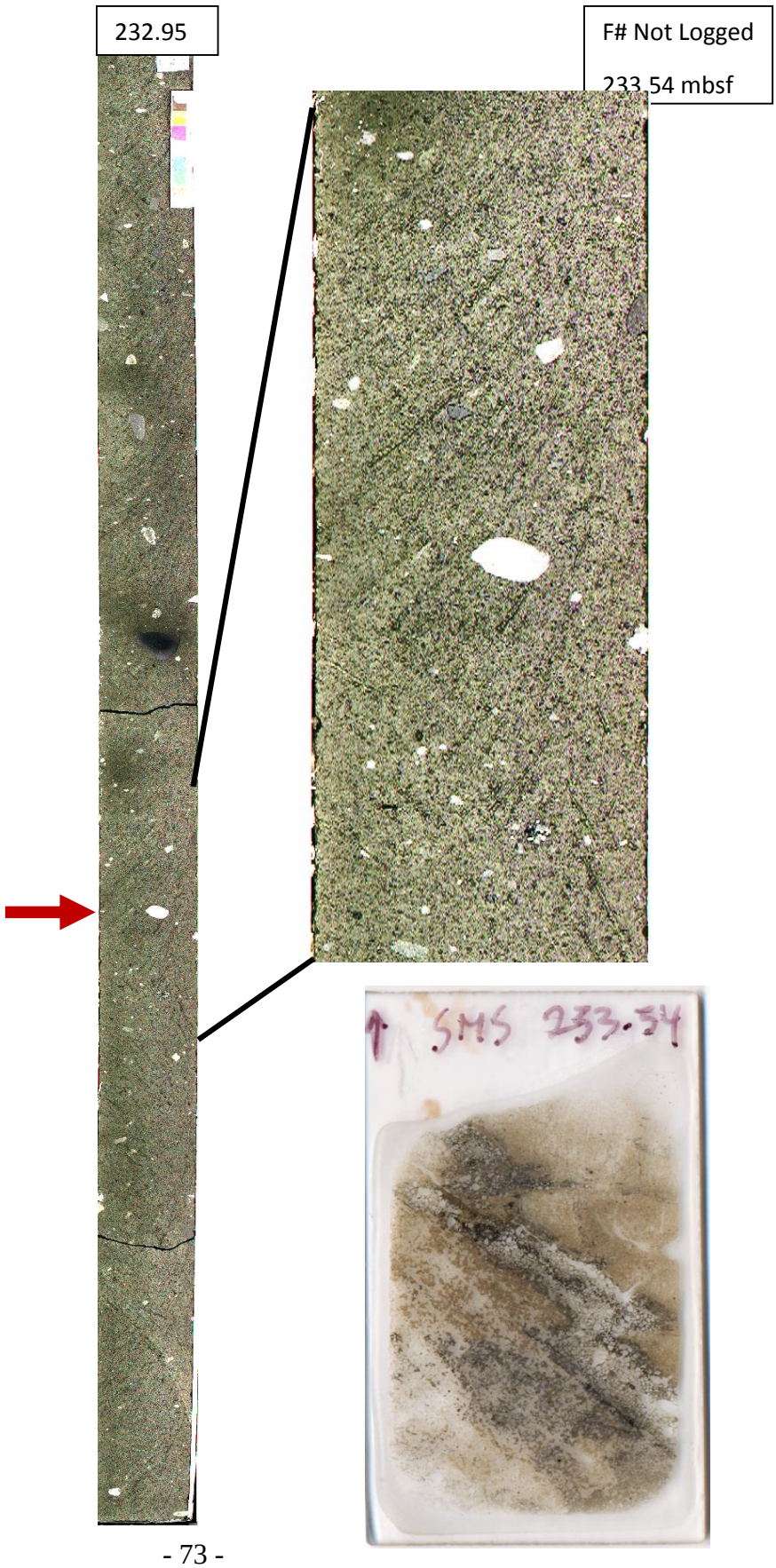
232.95
F# Not Logged
233.54 mbsf
SMS 233.54

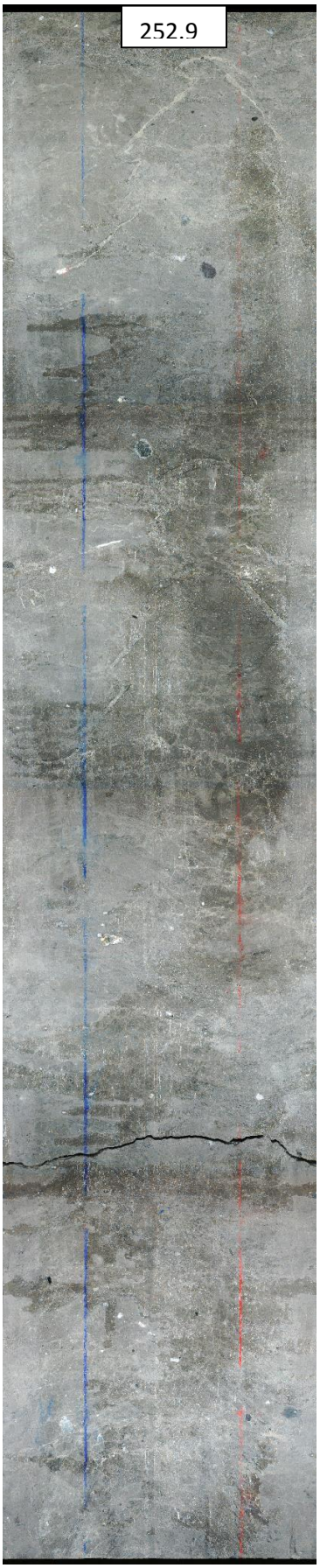



F# 1055b

253.47 mbsf

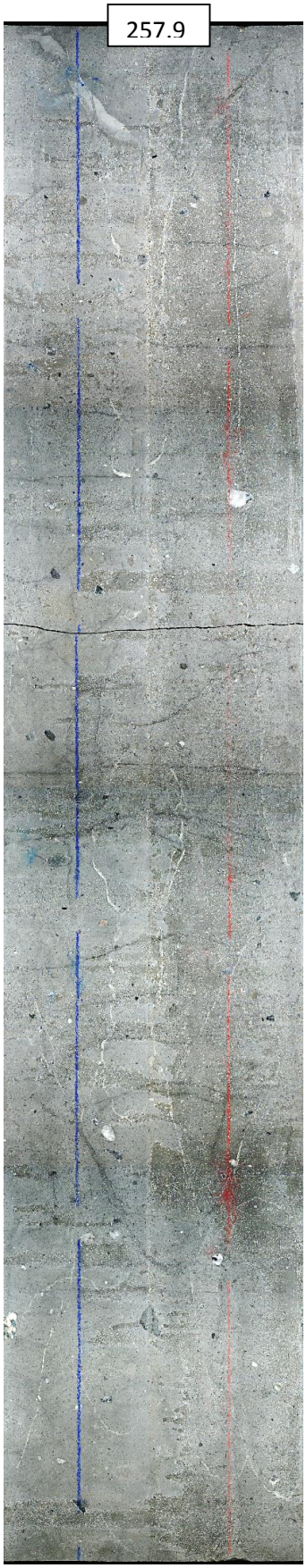



F# 1061b

257.99 mbsf

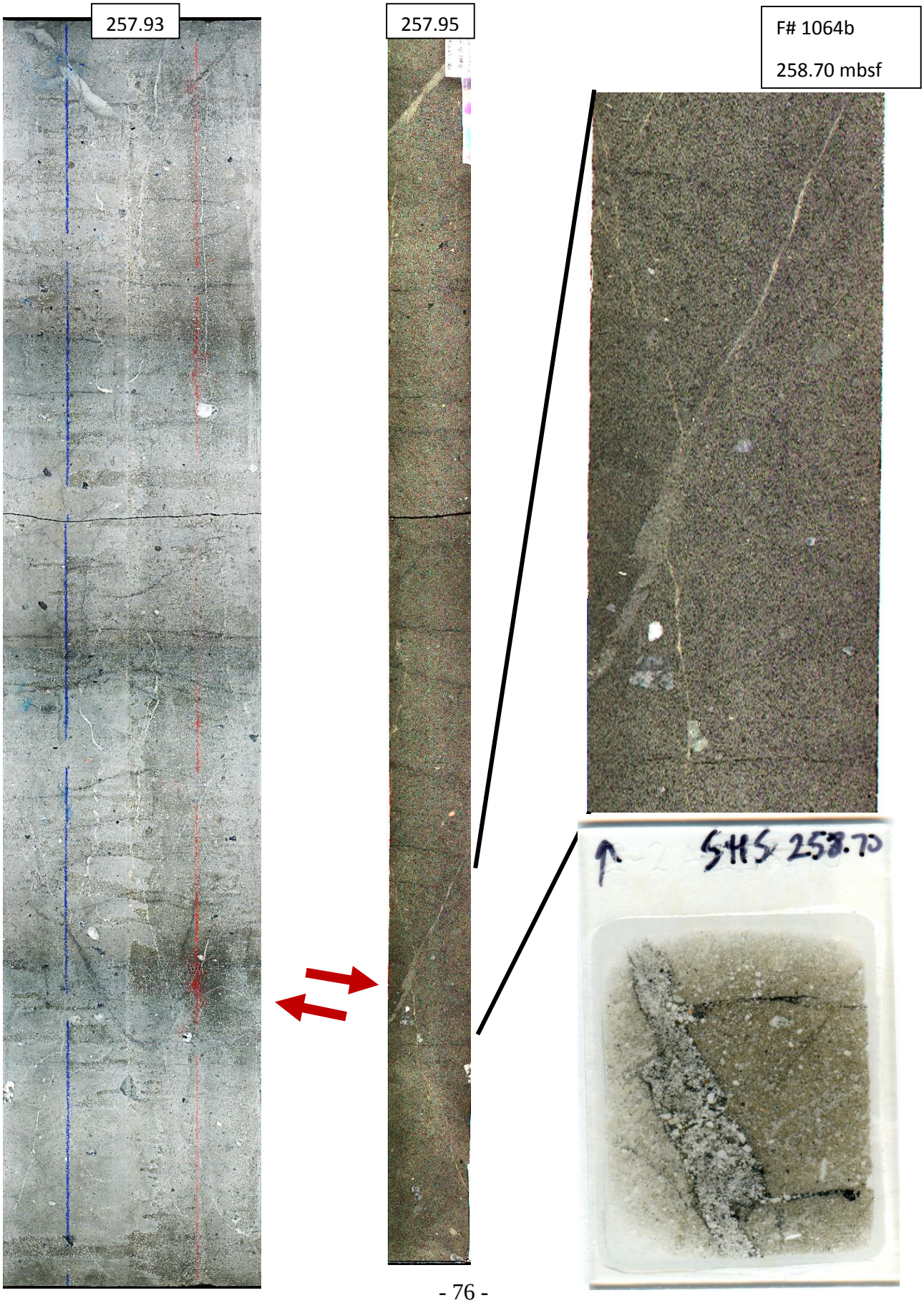
257.93
257.95
F# 1064b
258.70 mbsf
SHS 258.70



F# 1505

407.42 mbsf

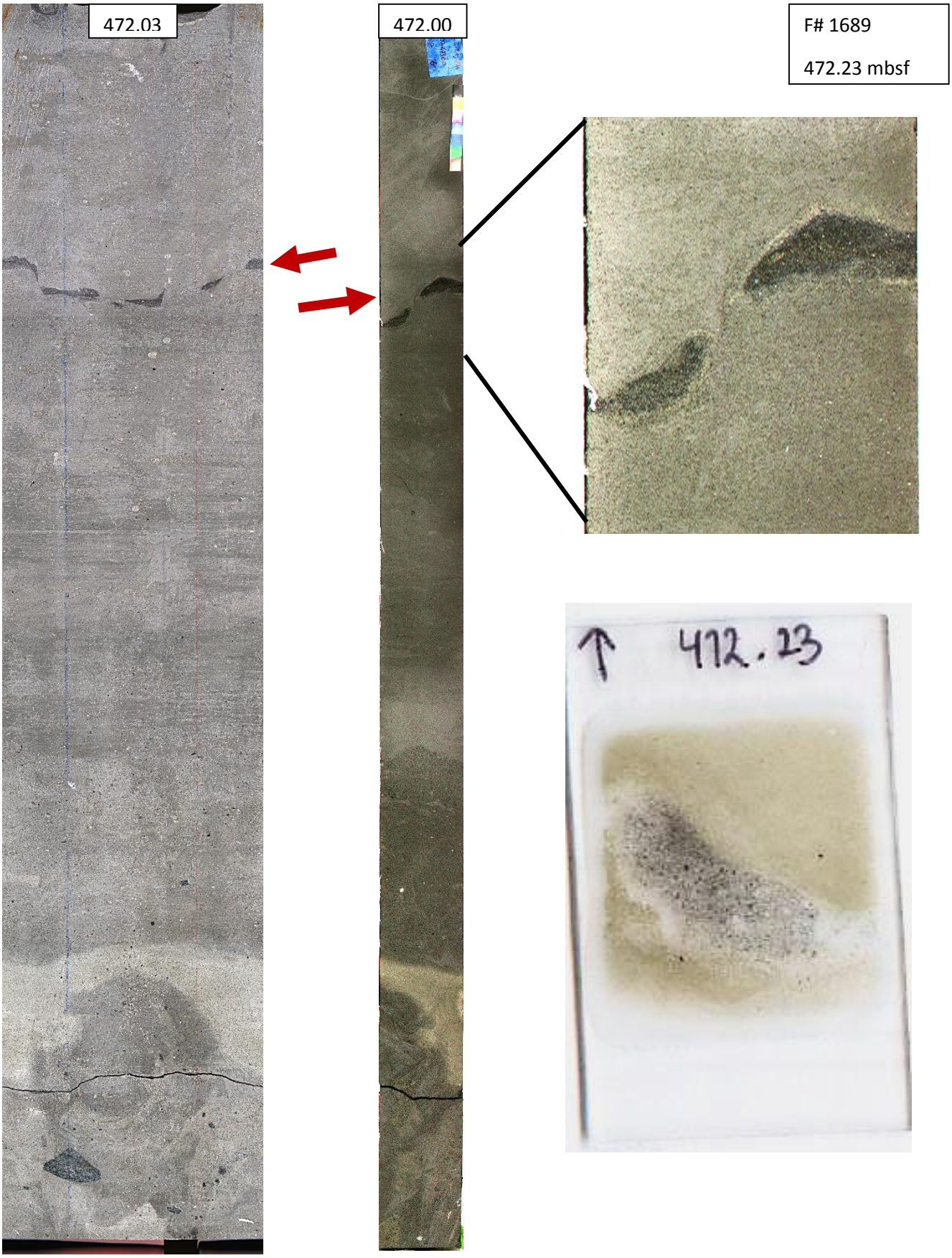
472.03
472.00
F# 1689
472.23 mbsf
↑ 472.23


514.99
514.92
F# Not Logged
515.78 mbsf
SHS 515.78

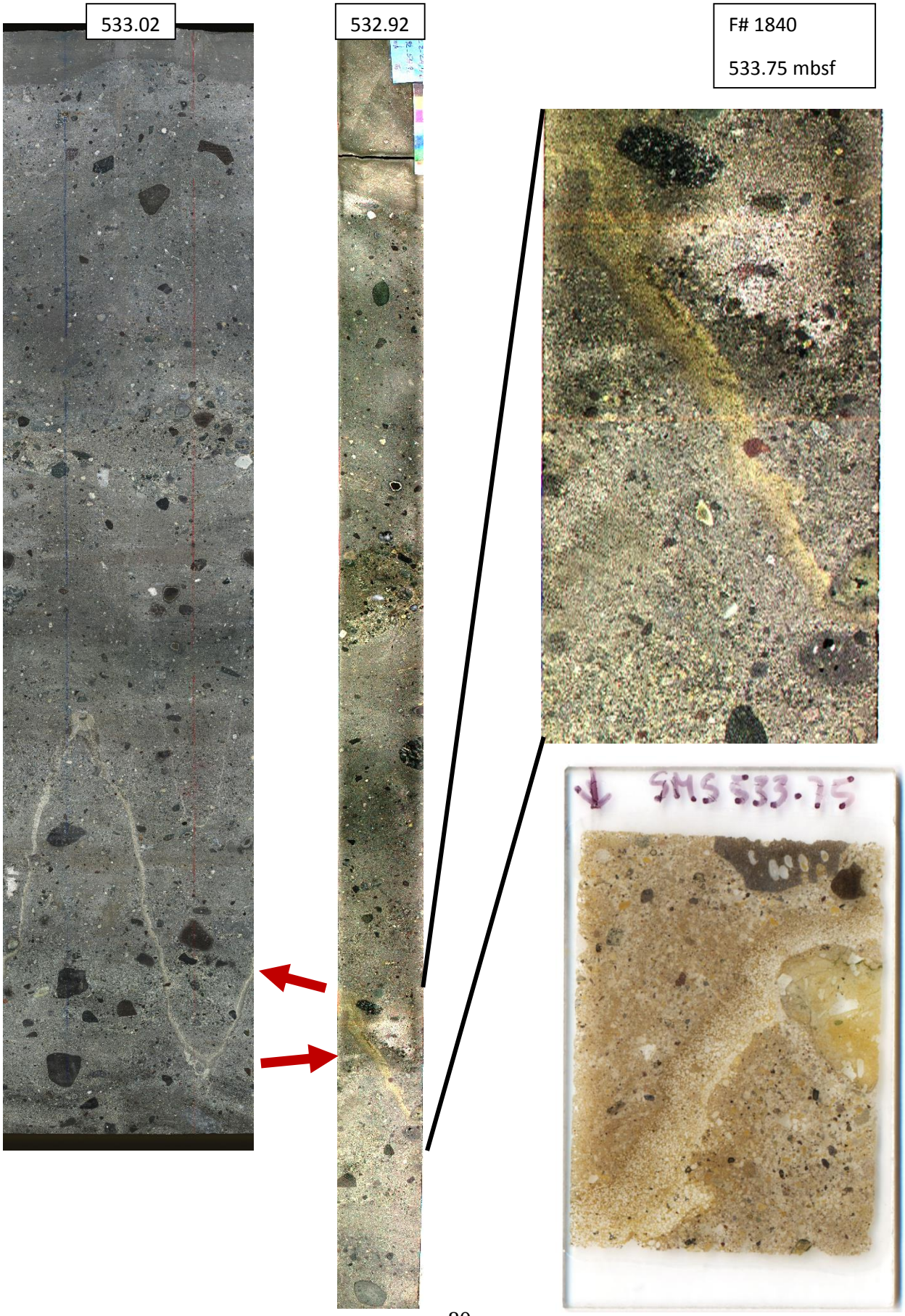
533.02
532.92
F# 1840
533.75 mbsf
SMS 533.75


574.92

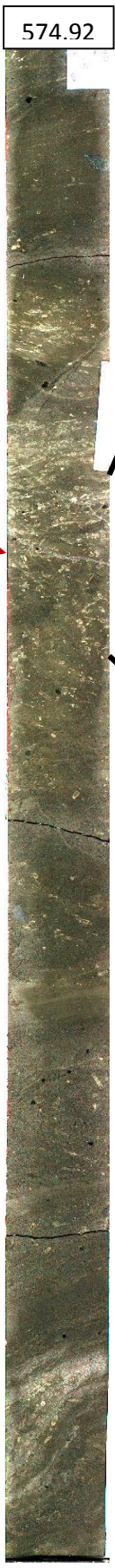
574.92


F# 1922
575.27 mbsf


← 5H5 575.27

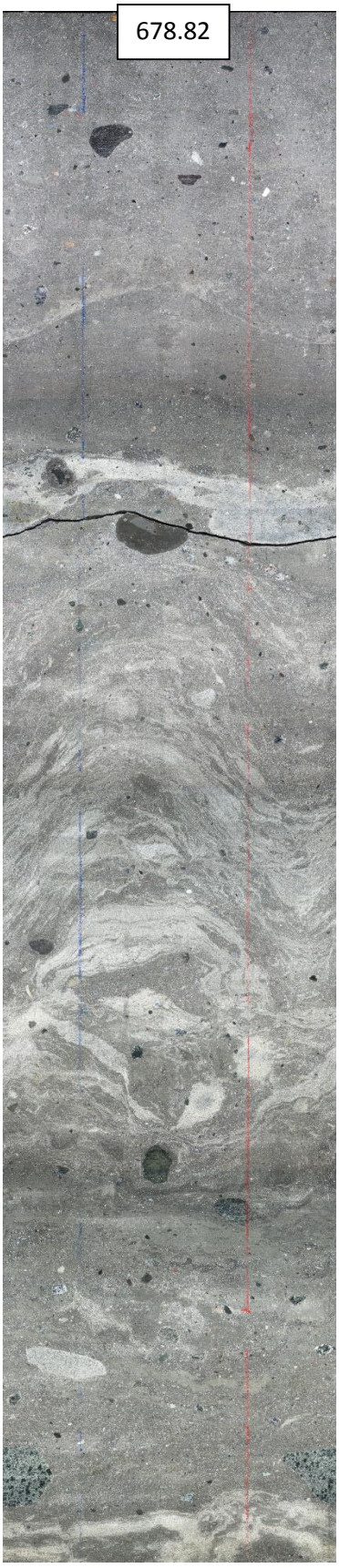



F# 2172

679.01 mbsf

# Appendix B: Stereoplots

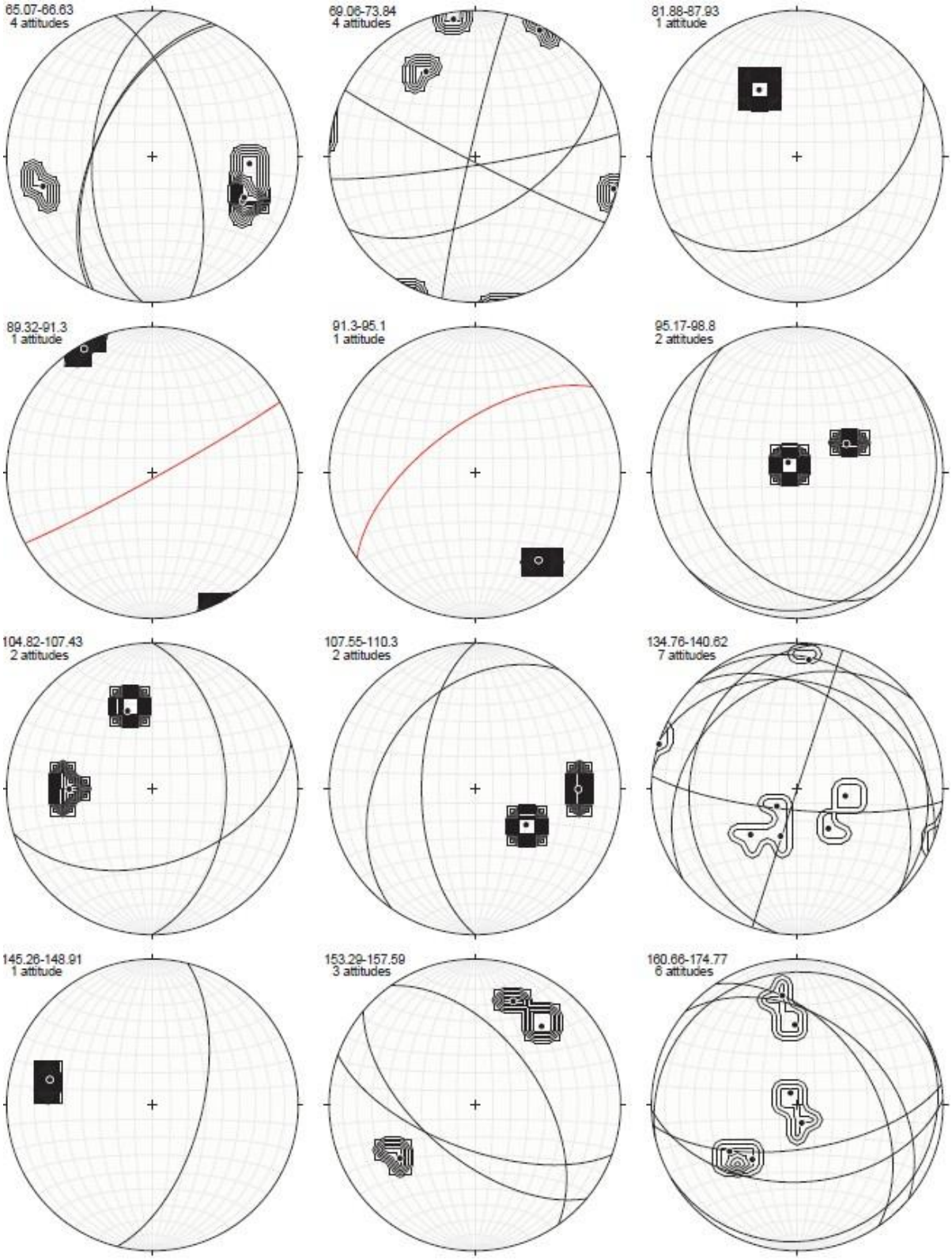

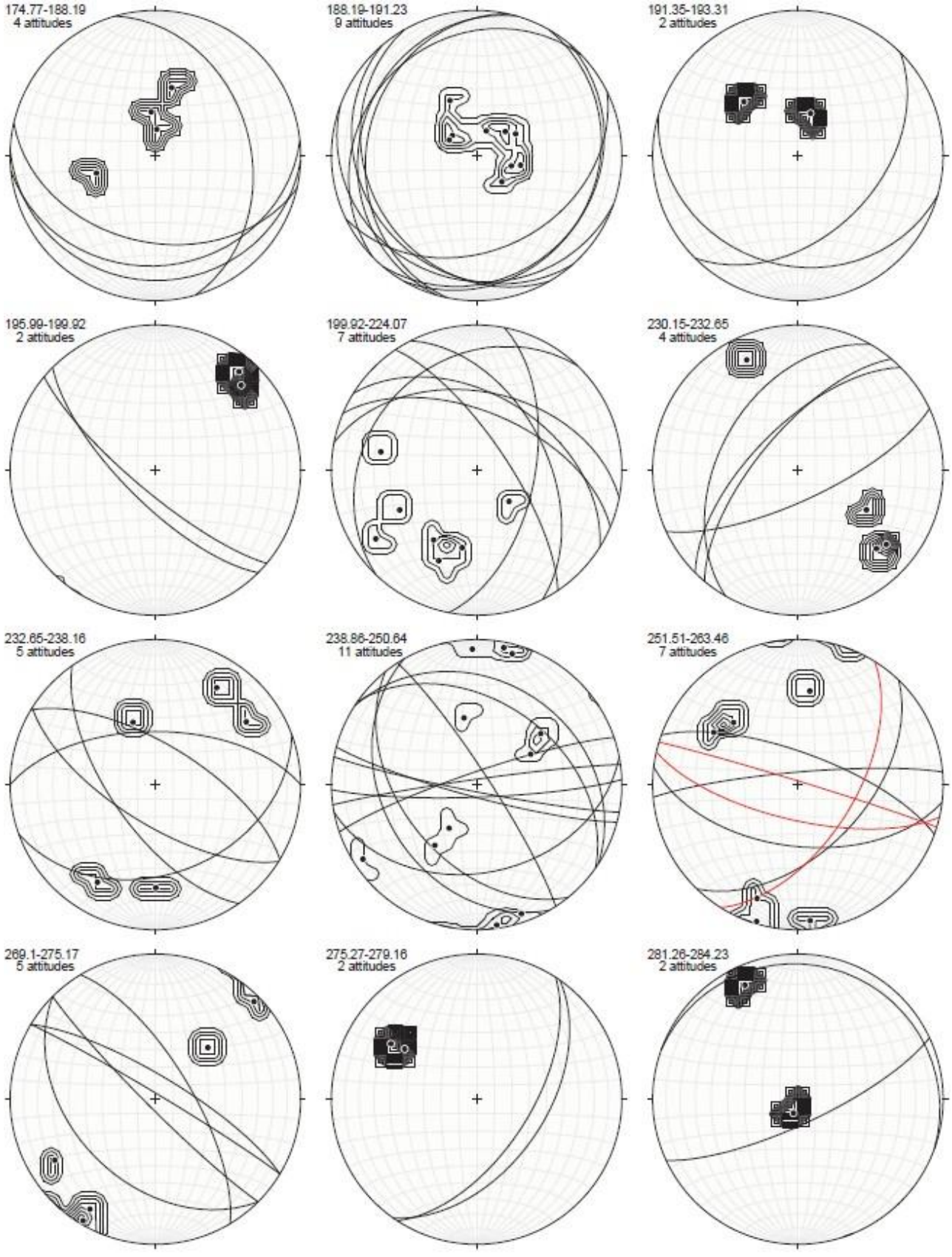
174.77-188.19
4 attitudes
188.19-191.23
9 attitudes
191.35-193.31
2 attitudes
195.99-199.92
2 attitudes
199.92-224.07
7 attitudes
230.15-232.65
4 attitudes
232.65-238.16
5 attitudes
238.86-250.64
11 attitudes
251.51-263.46
7 attitudes
269.1-275.17
5 attitudes
275.27-279.16
2 attitudes
281.26-284.23
2 attitudes

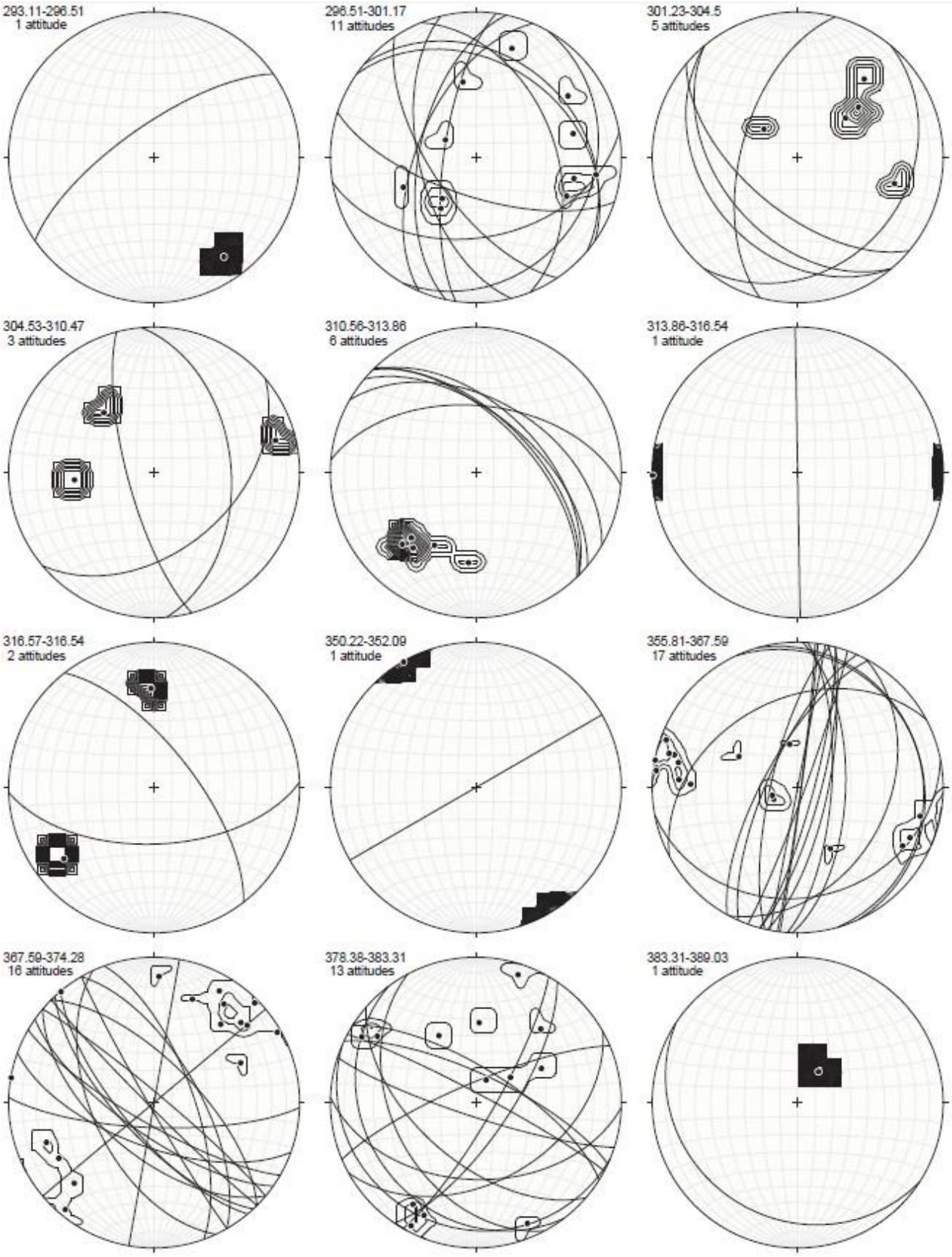
293.11-296.51
1 attitude
296.51-301.17
11 attitudes
301.23-304.5
5 attitudes
304.53-310.47
3 attitudes
310.56-313.86
6 attitudes
313.86-316.54
1 attitude
316.57-316.54
2 attitudes
350.22-352.09
1 attitude
355.81-367.59
17 attitudes
367.59-374.28
16 attitudes
378.38-383.31
13 attitudes
383.31-389.03
1 attitude

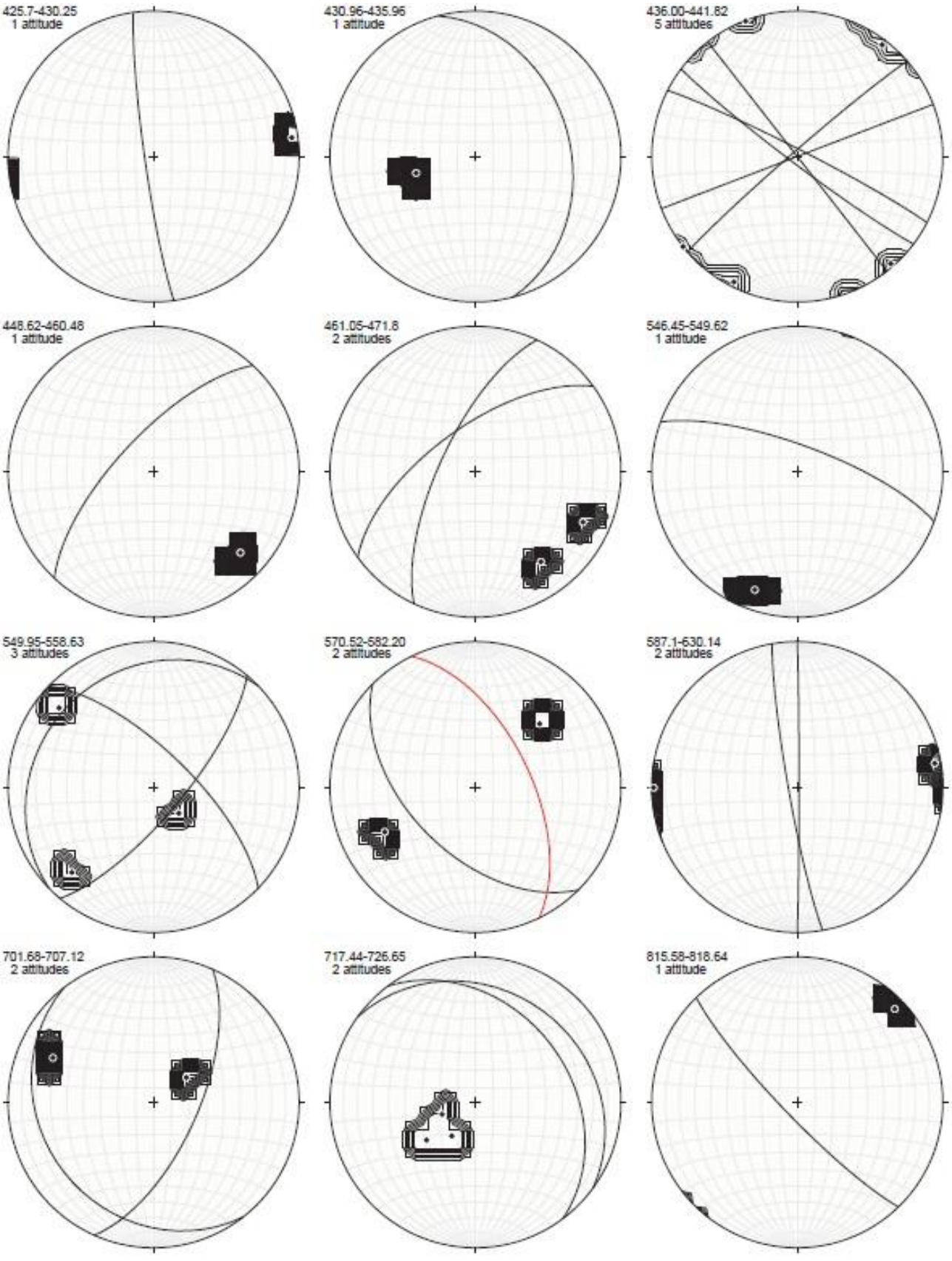
425.7-430.25
1 attitude
430.96-435.96
1 attitude
436.00-441.82
5 attitudes
448.62-460.48
1 attitude
461.05-471.8
2 attitudes
546.45-549.62
1 attitude
549.95-558.63
3 attitudes
570.52-582.20
2 attitudes
587.1-630.14
2 attitudes
701.68-707.12
2 attitudes
717.44-726.65
2 attitudes
815.58-818.64
1 attitude

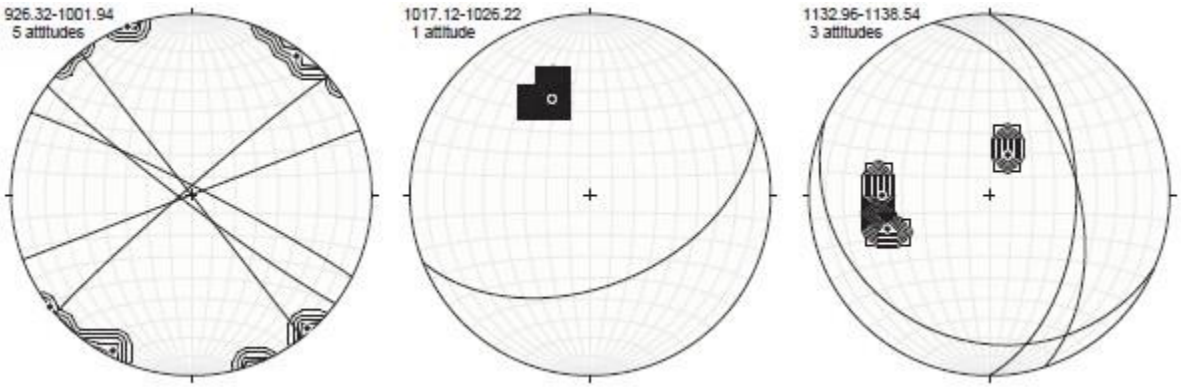
926.32-1001.94
5 attitudes
1017.12-1026.22
1 attitude
1132.96-1138.54
3 attitudes